

---

# PRIM: Meta-Learned Bayesian Root Cause Analysis

---

Christopher Lohse<sup>1,2</sup>  
lohsec@tcd.ie

Anish Dhir<sup>3</sup>  
anish.dhir.17@ucl.ac.uk

Amadou Ba<sup>2</sup>  
amadouba@ie.ibm.com

Bradley Eck<sup>2</sup>  
bradley.eck@ie.ibm.com

Marco Ruffini<sup>1</sup>  
marco.ruffini@tcd.ie

Jonas Wahl<sup>4,5</sup>  
jonas.wahl@dfki.de

<sup>1</sup>University of Dublin, Trinity College, Dublin, Ireland

<sup>2</sup>IBM

<sup>3</sup>Gatsby Computational Neuroscience Unit, University College London

<sup>4</sup>Deutsches Forschungszentrum für Künstliche Intelligenz (DFKI), Saarbrücken, Germany

<sup>5</sup>Department of Philosophy, University of Bergen, Norway

## Abstract

Root cause analysis (RCA) in complex systems is challenging due to error propagation across multiple variables, the need for structural causal knowledge, and the computational cost of inference at test time. We introduce PRIM (**P**rior-fitted **R**oot cause **I**dentification with **M**eta-learning), a causal meta-learning approach that frames RCA as a Bayesian inference task over a prior of causal models. By marginalising out structural uncertainty, PRIM implicitly finds changes in the data-generating mechanism between baseline and anomalous periods. In doing so, PRIM infers distributional differences without explicit statistical testing, and implicitly learns causal structure without model fitting at test time. Following the simulation-based meta-learning paradigm of prior-fitted networks, PRIM uses a Model-Averaged Causal Estimation (MACE) transformer neural process that jointly attends over observational and anomalous samples and the structural dependencies of nodes, enabling zero-shot inference in 17 ms for systems with up to 100 variables. Across synthetic benchmarks and two realistic benchmark datasets, PetShop and CausRCA, PRIM is competitive with methods that are aware of the system’s causal graphical structure a priori while outperforming graph-unaware methods on several tasks. Lightweight fine-tuning to specific domains and data dynamics improves performance further.

## 1 Introduction

In multivariate systems, anomalies rarely appear alone. When a fault occurs, its effects propagate through the system, causing multiple variables to behave abnormally simultaneously. Root cause analysis (RCA) is the task of identifying the original source of an error based on observations of the system both before and during the anomalous period [3]. RCA is a critical task across many domains, including cloud microservices [13; 40; 36], manufacturing [29], medicine[39; 28] as well as climate and sustainability [20; 2]. What makes RCA challenging is that, without knowledge of the causal structure, every anomalous variable is a possible root cause. Existing approaches address this

either by assuming knowledge of a causal graph describing the dynamics of the system [22; 4; 33] or by learning (parts of) a graph at inference time through causal discovery [17]. Both are costly: graph-based methods require accurate prior knowledge rarely available in practice, while methods that infer the graph at test time face computational costs scaling super-exponentially with the number of variables [7]. Statistical testing approaches such as  $\epsilon$ -diagnosis [40] and RCD [17] similarly become slower as the number of variables and data points grows. These approaches collapse graph and mechanism uncertainty into point estimates, but causal discovery is underspecified: from finite data and limited interventions, many graphs fit equally well, and committing to one risks misattributing the root cause.

A Bayesian, TNP(Transformer Neural Process)-based approach addresses these issues directly. Bayesian-model-averaging over graph and functional mechanism uncertainty mitigates the finite-sample and identifiability issues that affect point-estimate causal discovery [7; 27; 6] and attends over functional uncertainty over multiple models. The TNP collapses the usual two-step causal-discovery into RCA pipeline into a single inference step  $(D^{\text{obs}}, D^{\text{int}}, m) \rightarrow T$ , removing the need for explicit distribution-shift tests [40; 17; 13] and thus speeding up inference. We therefore reframe RCA as a Bayesian causal meta-learning problem [7; 8], following the simulation-based paradigm of prior-fitted networks [14; 30] that has proven effective for classification, anomaly detection [15], and time series forecasting [16], and showing that synthetic priors generalise to causal root cause analysis where labelled real-world data is scarce.

**Contributions** We introduce PRIM (**P**rior-fitted **R**oot cause **I**dentification with **M**eta-learning), a causal, non-graph-based method that scores candidate root cause nodes at zero-shot inference time given only normal and anomalous data as well as information where the anomaly has been observed. Intuitively, PRIM implicitly performs a test of distribution shift, identifying where the data-generating mechanism has changed between the observational and anomalous periods, but without any explicit statistical testing, instead averaging this reasoning through a meta-learned Bayesian posterior over graphs and functional mechanisms. PRIM achieves inference in 17 ms on an A100 GPU, making it practical for real-time fault diagnosis. For settings where the test distribution differs from the synthetic prior, PRIM can be fine-tuned in approximately three minutes on a single GPU. We evaluate on four synthetic setups and two realistic benchmarks, PetShop [13] and CausRCA [29], demonstrating robust general performance across well-supported settings and strong fine-tuned performance in more specialised cases.

## 2 Preliminaries

**Structural Causal Models** A Structural Causal Model (SCM) quantitatively represents causal relationships among multiple random variables and describes how changes in a system variable  $X$  lead to changes in other variables Pearl [35]. In an SCM, each variable  $X$  is assigned a value  $X := f_X(\text{pa}_X, \eta_X)$  through a function  $f$  of its *causal parents*  $\text{pa}_X$  and an independent noise term  $\eta_X$  Pearl [34]. Qualitative causal relationships in an SCM can be represented graphically as a Directed Acyclic Graph (DAG)  $\mathcal{G}$  with directed edges  $Z \rightarrow X$ ,  $Z \in \text{pa}_X$ . *Causal discovery* is the task to infer the structure of  $\mathcal{G}$  from observational or interventional data [42].

**Root Cause Analysis** Consider variables  $X = (X_1, \dots, X_n)$  whose causal interactions are given by an SCM with underlying DAG  $\mathcal{G} = (V, E)$ . Following Budhathoki et al. [3]; Ikram et al. [17] we define a **root cause** as a soft intervention on a subset of variables indexed by  $T \subseteq \{1, \dots, n\}$ , resulting in a shifted distribution  $P_X^T = \prod_{j \in T} \tilde{P}_{X_j | \text{pa}_j} \prod_{j \notin T} P_{X_j | \text{pa}_j}$ , where  $\tilde{P}_{X_j | \text{pa}_j}$  represents the modified conditional distribution for intervened variables. Following Eberhardt and Scheines [10], we distinguish between intervention types: a *hard intervention*  $do(X_i = x)$  replaces the mechanism  $f_i$  with a constant, eliminating the influence of  $\text{pa}(X_i)$ . In contrast, a *soft intervention* replaces  $f_i$  with a modified mechanism  $f'_i$ , altering the conditional distribution  $P(X_i | \text{pa}(X_i))$  without removing the causal edges from its parents. The *root cause analysis task* is to recover the intervention target set  $T$  given observational samples  $\mathcal{D}^{\text{obs}} = \{x^{(k)}\}_{k=1}^{n_{\text{obs}}} \sim P_X$  (normal operating conditions), interventional samples  $\mathcal{D}^{\text{int}} = \{x^{(k)}\}_{k=1}^{n_{\text{int}}} \sim P_X^T$  (anomalous conditions under intervention), and a symptom mask  $m \in \{0, 1\}^K$  with  $m_j = 1$  node  $j$  are the observed anomalies. Knowing  $m$  is needed for RCA since it restricts the set of interventions  $T$  to the anomaly we are interested in mitigating or we observed. Typically  $m$  only contains one node, the 'problem' or 'target' node [13], but it some

case it can also be several 'alarm nodes'[29]. In this paper we assume that we always know  $m$ , which is standard in most root cause analysis settings [13; 29]. Each sample  $x^{(k)} = (x_1^{(k)}, \dots, x_n^{(k)})$  is a realization of the variables  $X = (X_1, \dots, X_n)$ . In applied root cause analysis settings, the observational data corresponds to normal system behaviour, while the interventional data represents anomalous observations collected when the system is malfunctioning or degraded.

### 3 Bayesian Causal Root Cause Analysis

Dhir et al. [7, 8]; Robertson et al. [37] formalise causal discovery and inference as Bayesian meta-learning problems, training a neural process to approximate posteriors over causal structures from data. We adapt their formulation to RCA: rather than inferring  $\mathcal{G}$  or interventional distributions, our goal is to infer  $T$  directly, avoiding a two-step pipeline of causal discovery followed by RCA. In an SCM system, a soft intervention on  $T$  replaces rather than removes the functional mechanism  $f_T$ , leaving all other mechanisms unchanged. We define the mechanisms  $\mathbf{f}^{\text{obs}} = (\phi^{\text{obs}}, \epsilon^{\text{obs}})$  and  $\mathbf{f}^{\text{int}} = (\phi^{\text{int}}, \epsilon^{\text{int}})$  as tuples of functional mappings  $\phi$  and exogenous noise variables  $\epsilon$ . An intervention on target  $T$  can induce a shift in the functions, the noise distributions, or both, characterized by the mechanism change from  $\mathbf{f}^{\text{obs}}$  to  $\mathbf{f}^{\text{int}}$ . This change is localized to the intervention target:  $\mathbf{f}_i^{\text{int}} = \mathbf{f}_i^{\text{obs}}$  for all  $i \notin T$ , while  $\mathbf{f}_i^{\text{int}} \neq \mathbf{f}_i^{\text{obs}}$  for  $i \in T$ .

A Bayesian formulation of RCA averages over graphs rather than committing to a single estimated DAG, propagating structural uncertainty into the root cause posterior. By modelling  $\mathbf{f}^{\text{int}}$  as dependent on  $\mathbf{f}^{\text{obs}}$ , we exploit the fact that soft interventions preserve the graph and leave most structural equations unchanged, so  $\mathcal{D}^{\text{int}}$  also carries information about  $\mathbf{f}^{\text{obs}}$ .

**Bayesian Causal Model** In line with Dhir et al. [7, 8] adapted to the RCA setting, we define a *Bayesian causal model* (BCM) over the causal graph  $\mathcal{G}$ , the observational and interventional mechanisms  $\mathbf{f}^{\text{obs}}, \mathbf{f}^{\text{int}}$ , the corresponding data  $\mathcal{D}^{\text{obs}}, \mathcal{D}^{\text{int}}$ , the root cause set  $T$ , and the anomaly indicator  $m$ . The graph is drawn from  $\mathcal{G} \sim p_{\text{BCM}}(\mathcal{G})$ . Conditional on  $\mathcal{G}$ , we sample the observational mechanism  $\mathbf{f}^{\text{obs}} \sim p_{\text{BCM}}(\mathbf{f}^{\text{obs}} | \mathcal{G})$  and the root cause set  $T \sim p_{\text{BCM}}(T | \mathcal{G})$ . The interventional mechanism is then drawn as  $\mathbf{f}^{\text{int}} \sim p_{\text{BCM}}(\mathbf{f}^{\text{int}} | T, \mathbf{f}^{\text{obs}}, \mathcal{G}) = \prod_{i \in T} p_{\text{BCM}}(\mathbf{f}_i^{\text{int}} | \mathcal{G}) \prod_{j \notin T} \mathbb{1}_{\mathbf{f}_j^{\text{int}} = \mathbf{f}_j^{\text{obs}}}$ , reflecting that interventions modify only mechanisms or noises in  $T$  and leave others invariant. The random variables  $X^{\text{obs}}, X^{\text{int}}$  are distributed as  $X^{\text{obs}} \sim p_{\text{BCM}}(X^{\text{obs}} | \mathbf{f}^{\text{obs}})$ , respectively  $X^{\text{int}} \sim p_{\text{BCM}}(X^{\text{int}} | \mathbf{f}^{\text{obs}})$ , and the corresponding datasets are generated as i.i.d samples  $\mathcal{D}^{\text{obs}} = \{X^{\text{obs}(k)}\}_{k=1}^{n_{\text{obs}}}$ ,  $X^{\text{obs}(k)} \sim X^{\text{obs}}$  and  $\mathcal{D}^{\text{int}} = \{X^{\text{int}(k)}\}_{k=1}^{n_{\text{int}}}$ ,  $X^{\text{int}(k)} \sim X^{\text{int}}$ . Finally, the anomaly indicator  $m$  is sampled from the set of anomalous nodes  $\text{anom}(X^{\text{obs}}, X^{\text{int}}) := \{\ell \in V | p_{\text{BCM}}(x_\ell | \mathbf{f}^{\text{int}}) \neq p_{\text{BCM}}(x_\ell | \mathbf{f}^{\text{obs}})\}$  that change their marginal distribution (on a set of nonzero measure) after intervention,  $m \sim p(m | \text{anom}(X^{\text{obs}}, X^{\text{int}}))$ . Additionally, we assume that  $\text{desc}(T) \subseteq \text{anom}(X^{\text{obs}}, X^{\text{int}})^1$ , meaning that each descendant of the set  $T$  experiences a marginal distribution change. This can be considered a faithfulness assumption for root cause analysis as it precludes that the effect of the intervention cancels out along different paths to a descendant, 'coincidentally' reproducing the observational distribution. This assumption is implied by the  $\mathcal{I}$ -faithfulness assumption of [44] which is required for identifiability, see also Appendix A.2. As a consequence, this assumption allows us to sample  $m$  as  $m \sim p(m | \text{desc}(T))$ .

Defining  $\mathbf{f} \equiv (\mathbf{f}^{\text{obs}}, \mathbf{f}^{\text{int}})$ , the Bayesian posterior depends solely on the mechanism change, making separate component specifications redundant. The factorization of the distribution of the Bayesian Model gives the the following conditional independence statement: 1)  $T \perp X^{\text{obs}}, X^{\text{int}} | \mathbf{f}, m, \mathcal{G}$ : given the mechanism change, graph, and anomaly location, the data carry no additional information about  $T$ . (2)  $\mathcal{G} \perp m | X^{\text{obs}}, X^{\text{int}}$ , and (3)  $\mathbf{f} \perp m | \mathcal{G}, X^{\text{obs}}, X^{\text{int}}$ : the anomaly indicator carries no additional information about the graph or mechanism once  $X^{\text{obs}}, X^{\text{int}}$  are known. Thus, we define the Bayesian posterior over the root cause (derived in Appendix A.1) as

$$p(T | \mathcal{D}^{\text{obs}}, \mathcal{D}^{\text{int}}, m) = \sum_{\mathcal{G}} \int p(T | \mathbf{f}, \mathcal{G}, m) p(\mathbf{f} | \mathcal{G}, \mathcal{D}^{\text{obs}}, \mathcal{D}^{\text{int}}) p(\mathcal{G} | \mathcal{D}^{\text{obs}}, \mathcal{D}^{\text{int}}) d\mathbf{f}, \quad (1)$$

which marginalises over graph and functional mechanism uncertainty. Conditioning on  $m$  helps the the posterior to assign scores to any node whose mechanism has changed that lead to a direct shift at

<sup>1</sup>Observe that the converse inclusion  $\text{desc}(T) \supseteq \text{anom}(X^{\text{obs}}, X^{\text{int}})$  holds by construction of our BCM.

$m$ . This posterior is intractable: the sum over  $\mathcal{G}$  is exponential in  $|V|$  and the integral over  $\mathbf{f}$  is over an infinite-dimensional function space.

Following Dhir et al. [8, 7]; Robertson et al. [37], we therefore amortise inference with a meta-learned model  $f_\theta$ , trained on synthetic *BCM* samples, that directly scores candidate root cause nodes

$$p_\theta(T = j \mid \mathcal{D}^{\text{obs}}, \mathcal{D}^{\text{int}}, m) = \text{softmax}(f_\theta(\mathcal{D}^{\text{obs}}, \mathcal{D}^{\text{int}}, m))_j, \quad j \in V. \quad (2)$$

Although  $p(\mathcal{G} \mid \mathcal{D}^{\text{obs}})$  may remain diffuse over the observational Markov equivalence class,  $p_\theta(T \mid \mathcal{D}^{\text{obs}}, \mathcal{D}^{\text{int}}, m)$  can still identify  $T$ . Following Squires et al. [44], assuming an acyclic SCM, causal sufficiency, mechanism invariance for non-targets, and  $\mathcal{I}$ -faithfulness (see Appendix A.2),  $\mathcal{D}^{\text{obs}}$  and  $\mathcal{D}^{\text{int}}$  together with the anomaly  $m$  identify the root-cause set  $T$  even though the underlying DAG itself may not be uniquely recoverable. Bayesian model averaging is therefore well-suited to this setting: it correctly propagates the residual graph ambiguity into the posterior over  $T$ , which remains concentrated on the true root cause set.

## 4 Related Work

**Transformer Neural Process and Prior-Fitted Networks** Since estimating the posterior over graph and functional uncertainty is hard, we use a Transformer Neural Process (TNP) trained as a Prior-Fitted Network (PFN), an approach proven effective on similar problems [14; 15; 9; 7; 37] across diverse domains [31; 11; 1]. PFN refers to the training paradigm: learning to approximate the posterior predictive by fitting to samples drawn from a synthetic prior. TNP refers to the architecture, a Neural Process built on the transformer [47]. Trained this way, PFNs learn general tabular representations with strong out-of-distribution performance on regression and classification [14; 16; 30], can be fine-tuned to new distributions [16], and as Neural Processes produce uncertainty-aware estimates at inference without intermediate steps such as explicit graph estimation [8]. They have been applied to causal discovery [9] and effect estimation [8; 37]; in particular, Dhir et al. [8]; Robertson et al. [37] use a TNP to estimate interventional distributions given an intervention target, making it a natural foundation for estimating  $T$  directly from  $\mathcal{D}^{\text{obs}}$ ,  $\mathcal{D}^{\text{int}}$ , and  $m$  without a separate causal discovery step. Using a Bayesian TNP avoids two-step algorithms that first fix a graph and then perform RCA, instead inferring  $T$  jointly with  $\mathcal{G}$  and the mechanisms. Further, it does not rely on statistical distribution difference tests to detect mechanism changes, which are often underpowered under limited interventional data.

**Root Cause Analysis** RCA closely aligns with intervention target estimation [19; 45; 46; 49; 44]: in both, interventions on a small set of nodes explain shifts in the overall distribution, and the goal is to identify these nodes. It has been applied to cloud microservices [41; 5; 24; 40; 25; 22; 36; 23; 13], manufacturing [29], medicine [39; 28], and sustainability [20; 2].

Existing approaches differ in whether they assume a known causal graph, and most impose some form of parametric assumptions on the mechanism family. *Graph-based* methods include Traversal [13], which selects the highest-ranked anomalous node with no anomalous parent connected to  $m$ ; CIRCA [22], which fits a linear Gaussian SCM and tests which conditional has changed; counterfactual attribution via Shapley values [4]; PageRank [33]; and CausTR [29], which ranks variables by causal proximity to alarm activations. *Graph-free* methods relax this requirement but typically introduce others: RCD [17] performs local causal discovery under unknown soft interventions [19; 44], extended to partial structural knowledge [18];  $\varepsilon$ -diagnosis [40] uses two-sample tests; BARO [36] ranks by deviation magnitude; TimeRank by recency of value changes; and Meta-RCA [23] combines LLMs with a Bayesian belief model and a LLM-determined knowledge Graph. A recent line tackles the harder *single-sample* regime [21; 32; 38] under linear-SEM assumptions; we instead address the multi-sample setting with modelling functional and structural uncertainty.

PRIM aims to address both points: it is graph-free yet retains a probabilistic treatment of causal structure by Bayesian-model-averaging over graph and functional uncertainty rather than committing to either. The TNP architecture enables direct inference  $(\mathcal{D}^{\text{obs}}, \mathcal{D}^{\text{int}}, m) \rightarrow T$  without an intermediate causal discovery step, following the training paradigm of TabPFN [14; 30], where training on synthetic prior data alone matches or exceeds task-specific baselines on real-world tabular tasks also adapted to anomaly detection [15] and time series forecasting [16]. PRIM applies this to RCA by meta-learning a TNP on synthetic BCM samples [7; 8; 37; 15], reducing the need for test-time statistical testing or parametric SCM assumptions.

## 5 Prior and Model Architecture

### 5.1 Prior and Episode Structure

For training PRIM each training episode samples a random causal DAG (Erdős–Rényi, Barabási–Albert, or bipartite) over  $K \sim \text{Unif}(K_{\min}, K_{\max})$  nodes with expected in-degree  $\bar{d} \sim \text{Unif}(1.8, 2.5)$ . Structural equations are drawn uniformly from five mechanism families: linear, weighted tanh, neural network, Gaussian process, and constant-baseline. The constant baseline remains at the same value and only changes during anomalous periods. We model each mechanism with heteroscedastic or family-specific noise. Given a fixed DAG and SCM, each episode draws  $n_q$  independent scenarios from  $\mathcal{M}$ :  $\{(\mathcal{D}_i^{\text{obs}}, \mathcal{D}_i^{\text{int}}, T_i, m_i)\}_{i=1}^{n_q}$ .

We write  $\mathcal{M} = (\mathcal{G}, f)$  for a sampled SCM instance, consisting of a DAG  $\mathcal{G}$  and its associated structural equations  $f = \{f_i\}_{i \in \mathcal{V}}$ . Each scenario samples unique observational data  $\mathcal{D}^{\text{obs}}$  with  $n_{\text{obs}} \sim \text{Unif}(5, 500)$ , applies a random intervention at a non-leaf node  $T_i$  via weight-change (only for Neural Network Prior) in the function and or function change (80%), additive shift (15%), or hard do-intervention (5%), and generates  $\mathcal{D}^{\text{int}}$  with  $n_{\text{int}} \sim \text{Unif}(1, 200)$ . The symptom mask  $m_i$  is set to  $T_i$  itself or a uniformly sampled descendant. After sampling, data are z-scored using the observational statistics and clipped to  $\pm 10$  to bound the dynamic range to a level consistent with real-world monitoring signals, then zero-padded to  $K_{\max}$  nodes. Full data generation and distributional details are provided in Appendices B.2 - B.1.

### 5.2 Model Architecture

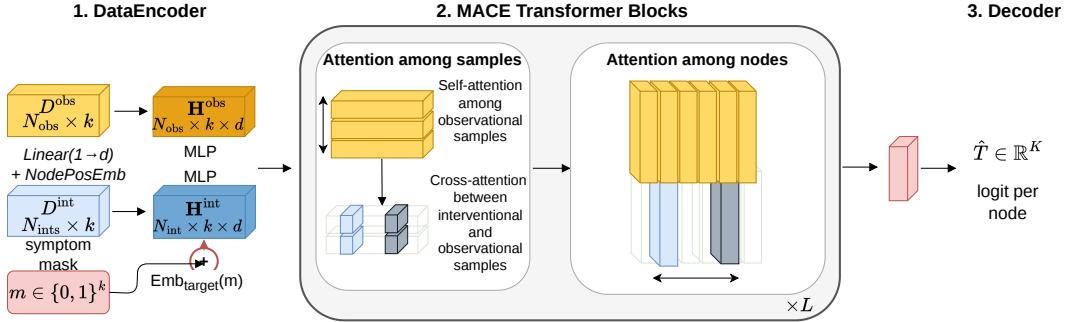


Figure 1: PRIM architecture.  $L$  MACE-TNP blocks refine obs/int embeddings via alternating sample- and node-level attention. The difference  $\Delta = \bar{\mathbf{H}}^{\text{int}} - \bar{\mathbf{H}}^{\text{obs}}$  is decoded to per-node logits  $\hat{T} \in \mathbb{R}^K$ .

Our model, PRIM (Prior-fitted Root cause Identification with Meta-learning), is built around the MACE-TNP architecture introduced by Dhir et al. [8] for estimating interventional distributions. While the original MACE-TNP model conditions on a target and observational distribution, our formulation receives both observational (normal) and interventional (anomalous) data and predicts which node was intervened on, i.e. the root cause. An overview of the architecture is shown in Figure 1. Variable graph sizes are handled by zero-padding and attention masking following Hollmann et al. [14, 15]; implementation details are given in Appendix B.3.

**Data Encoding** Observational and interventional datasets  $\mathcal{D}^{\text{obs}} \in \mathbb{R}^{n_{\text{obs}} \times K}$ ,  $\mathcal{D}^{\text{int}} \in \mathbb{R}^{n_{\text{int}} \times K}$  are encoded by separate DataEncoders into tensors  $\mathbf{H}^{\text{obs}} \in \mathbb{R}^{n_{\text{obs}} \times K \times d}$ ,  $\mathbf{H}^{\text{int}} \in \mathbb{R}^{n_{\text{int}} \times K \times d}$ . Each scalar  $x_{s,k}$  is linearly projected and summed with a learned node positional embedding:  $\mathbf{H}_{s,k} = Wx_{s,k} + \mathbf{e}_k^{\text{node}}$ , where  $W \in \mathbb{R}^{d \times 1}$  and  $\mathbf{e}_k^{\text{node}} \in \mathbb{R}^d$  are learned parameters shared across samples. For the binary symptom mask  $m \in \{0, 1\}^K$  a learned target embedding is added to  $\mathbf{H}^{\text{int}}$  at each sample position.

**MACE Transformer Blocks**  $L$  stacked layers refine the paired embeddings via three attention operations: (1) obs self-attention: for each node  $k$ , observational samples attend to one another; (2) int→obs cross-attention: interventional samples attend to observational samples as keys/values; (3) node self-attention: all samples jointly attend across the  $K$  node positions. Each operation is

followed by a residual connection and layer normalisation; a shared Multi Layer Perceptron (MLP) closes each block.

**Decoding** After  $L$  layers, both streams are mean-pooled over samples and differenced:

$$\Delta = \frac{1}{n_{\text{int}}} \sum_s \mathbf{H}_s^{\text{int}} - \frac{1}{n_{\text{obs}}} \sum_s \mathbf{H}_s^{\text{obs}} \in \mathbb{R}^{Kf \times d} \quad (3)$$

This tells the model to consider the difference between the two distributions for classifying  $T$ , implicitly performing the distributional difference test. Learned pooling variants were explored but did not improve over the fixed mean within the training budget available; we leave this to future work. A two-layer MLP decoder then maps each node embedding to a logit:  $\hat{T} = c_\psi(\Delta) \in \mathbb{R}^K$ .

**Training Objective** The model is trained on synthetic SCMs drawn from  $p(\mathcal{M})$ . For each  $(\mathcal{D}^{\text{obs}}, \mathcal{D}^{\text{int}}, T) \sim \mathcal{M}$ , we minimize the loss  $\mathcal{L} = \mathbb{E}_{\mathcal{M}} \mathbb{E}_{T, \mathcal{D} | \mathcal{M}}[\ell(c_\psi(\Delta), T)]$ , where  $\ell(\hat{y}, y) = -\sum_k y_k \log \hat{y}_k$  is the cross-entropy between  $\hat{y} = \text{softmax}(\hat{T})$  and the one-hot target  $y$ .

**Finetuning** Although PRIM can be deployed zero-shot, performance on a specific target system can be improved through fine-tuning with a prior that better matches the posterior distribution, cf. [16]. We consider two setups: *full-model* fine-tuning, where all parameters are updated, and *decoder-only* fine-tuning, where the backbone is frozen and only the final MLP decoder is tuned. When the posterior distribution is close to the training prior decoder-only fine-tuning suffices, as we assume that the model already produces well-calibrated node embeddings and only the mapping from  $\Delta$  to the root-cause logits  $\hat{T}$  requires adaptation. For stronger out-of-distribution generalization, full-model fine-tuning provides additional gains, particularly when interventional samples are scarce. For the considered real-world benchmarks, we adopt decoder-only fine-tuning, as we expect the target distributions to not deviate strongly from the training prior. We verify these claims empirically in Appendix D.2.

## 6 Experiments

We evaluate PRIM on three synthetic setups and two real-world benchmarks, comparing against methods used in the PetShop benchmark [13] with available implementations. We exclude Counterfactual attribution (prohibitive runtime), Meta-RCA (LLM dependency, no public code), and TimeRank, CausTR, and Baro (require time-series data absent from our synthetic setup). We train three model sizes on synthetic SCM data (Section 5.1): PRIM-S ( $K_{\text{max}} = 5$ ), PRIM-M ( $K_{\text{max}} = 10$ ), and PRIM-L ( $K_{\text{max}} = 100$ ), each with  $\sim 4\text{M}$  parameters; see Appendix C for architecture, training, and compute details, and Table A.2 for the model used per experiment. We measure single-root-cause performance by Recall@ $k$  (1 if the true cause is in the top- $k$  predictions, 0 otherwise) and multi-root-cause performance by MAP@ $k$ , which accounts for the ranking quality of all true causes.

### 6.1 Synthetic Data

We consider three controlled setups of increasing complexity, adapting Dhir et al. [8]’s structure to the RCA setting: a three-node mediator/confounder scenario testing structural ambiguity, a scalability analysis across graph sizes, and a multi-root-cause scenario testing transfer from single- to multi-fault identification. We report 90% bootstrap confidence intervals (500 resamples) over 200 episodes. We evaluate under two mechanisms commonly used in this setting [8]: Neural Network (NN) and Gaussian Process (GP). Soft-interventions are implemented by perturbing the intervened node’s weights (NN) or noise parameters (GP); we do not consider hard-interventions here. Appendix D.1 provides an additional sanity-check setup with a graph not identifiable from observational data.

**Confounder and Mediator** We test on two three-node structures shown in Figure 2: a mediator and a confounder, with  $X$  always the root cause. This tests whether PRIM correctly attributes the root cause in the presence of indirect causal paths and common causes. We use  $n_{\text{int}} = 10$  anomalous samples, varying  $n_{\text{obs}}$  for the cross-model comparison and varying  $n_{\text{int}}$  with  $n_{\text{obs}} = 100$  fixed to isolate PRIM’s sensitivity to each.

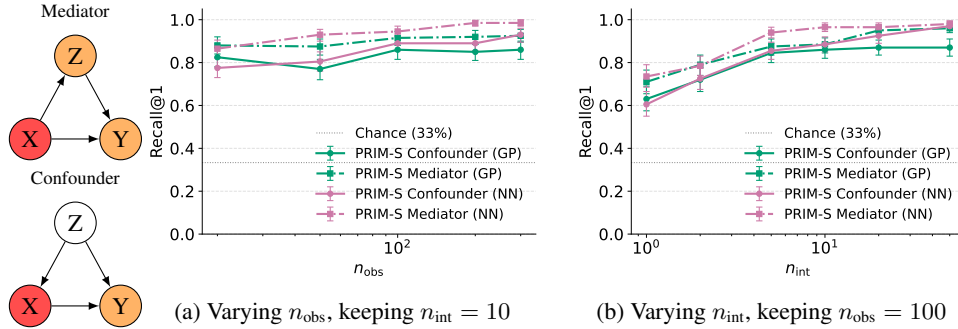
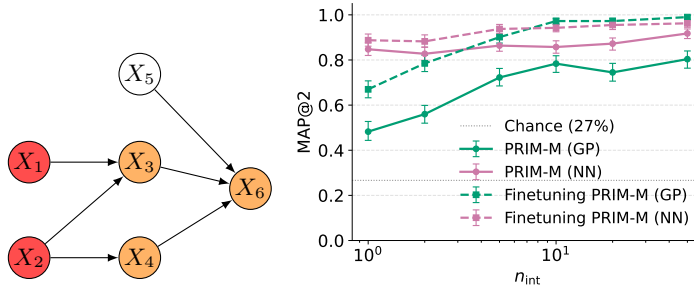


Figure 2: Three-node confounder vs. mediator scenario. X (■ red) is the root cause; downstream nodes (■ orange) are descendants; unaffected nodes are white.

Figure 2 shows results at  $n_{obs} = 100$ ,  $n_{int} = 10$ . A comparison with other methods over different number of observational data can be found in Appendix D.3. In summary PRIM achieves the best performance among graph-not-given methods for  $n_{obs} = 100$  across all settings, with RCD as the closest competitor, both slightly below graph-given methods where access to the true causal structure provides a clear advantage. The confounder structure proves harder than the mediator for all graph-not-given methods, while graph-given methods are unaffected. GP mechanisms are harder than NN across the board, as NN functional mechanisms produce more distinctive distribution shifts in our setup whereas GP mechanisms change only the noise structure. As shown in Figure 2b, increasing  $n_{int}$  has a stronger effect on performance than increasing  $n_{obs}$ .

**Multi-Root Cause Identification** Here PRIM’s ability to identify multiple simultaneous root causes on the fixed DAG shown in Figure 3 is tested, where two independent nodes  $X_1$  and  $X_2$  are intervened upon simultaneously. Performance is measured by MAP@2, requiring both root causes to appear in the top-2 predictions, testing zero-shot transfer from single to multi-fault identification. The fine-tuned variant is trained on 1,600 synthetic multi-fault scenarios with mixed NN/GP mechanisms and full-model fine-tuning; details are given in Appendix C.



(a) Varying  $n_{int}$ , keeping  $n_{obs} = 100$

Figure 3: Multi-root-cause evaluation on a 6-node DAG (left).  $X_1, X_2$  (■ red) are root causes;  $X_3, X_4, X_6$  (■ orange) are descendants;  $X_5$  (white) is unaffected. MAP@2 measures whether both appear in the top-2 predictions. Solid: zero-shot; dashed: finetuned on multi-fault DAGs.

As shown in Figure 3 for a fixed  $n_{obs} = 100$ , the fine-tuned variant substantially outperforms the base model, with gains becoming more pronounced as  $n_{int}$  increases and GP mechanisms are handled more reliably. Notably, even the base model exceeds the random MAP@2 baseline of  $\approx 0.27$  with sufficient interventional samples, suggesting that single-fault training transfers partially to the multi-fault setting.

**Different Node Sizes** To assess scalability, we evaluate PRIM across randomly sampled DAGs of varying size at  $n_{obs} = 100$  and  $n_{int} = 10$ , with performance measured by Recall@1 (Figure 4). We also include PC-versions of graph-based methods (PC-Traversal, PC-CIRCA), where the causal

graph is estimated via the PC algorithm [43] with maximum conditioning set depth 3, providing graph-free variants of these methods for a fair comparison.

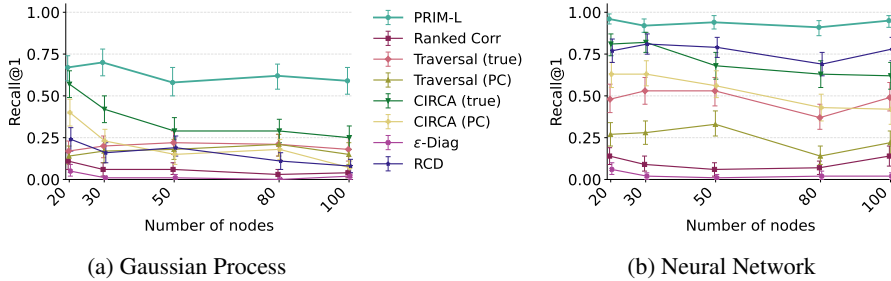


Figure 4: Recall@1 vs. number of nodes at  $n_{\text{obs}} = 100$ ,  $n_{\text{int}} = 10$ .

As highlighted in Figure 4 PRIM outperforms all baselines in both GP and NN settings, including methods with access to the ground truth graph, and its Recall@1 degrades more slowly with increasing graph size than any other method. As noted previously, GP data is harder across the board due to weaker distributional shifts compared to NN weight-change interventions. CIRCA is the strongest competitor in the GP setting, while for NN data CIRCA leads for smaller graphs (up to  $\sim 20$  nodes) and RCD becomes competitive at larger sizes. The PC-based variants are substantially worse than their True-graph counterparts, likely due to nonlinear functional mechanisms that violate the assumptions of the executed version of the PC algorithm, even though they still outperform RCD and  $\epsilon$ -diagnosis (which also assume linear relationships) in both settings. The full results over different observational sizes and the medium model can be found in Appendix D.4.

Since inference time is crucial for real-world deployment, we benchmarked all methods across node sizes. PRIM stays constant at 17ms (large model) as it requires only a single forward pass, while other methods scale exponentially. Traversal is slightly faster up to 50 nodes when given the causal graph, but much slower once causal discovery is included. Full results are in D.5. On a MacBook Pro M3 Max, PRIM runs in  $\sim 280$ ms on CPU and  $\sim 35$ ms on MPS GPU across all node sizes.

## 6.2 Realistic Data with unknown Distribution

We evaluate on two real-world benchmarks spanning cloud microservices and manufacturing. The PetShop benchmark [13] (CC Public License) is a microservice dataset based on the AWS Observability Workshop comprising  $\sim 44$  services monitored via latency and availability metrics, with 48 fault injection issues across four traffic scenarios, each with a single root cause.  $\mathcal{D}^{\text{obs}}$  covers the normal baseline period ( $|\mathcal{D}^{\text{obs}}| \in \{589, 1652\}$  depending on scenario) and  $\mathcal{D}^{\text{int}}$  the anomaly period ( $|\mathcal{D}^{\text{int}}| = 5$  five-minute snapshots); the symptom mask  $m$  indicates the entry-point service (PETSITE). The CausRCA benchmark [29] (Apache License 2.0) is a partially real, partially simulated factory system with 100 runs across 19 fault injection experiments in three subsystems (probe: 34, coolant: 25, hydraulics: 41), featuring multiple simultaneous root causes; all firing alarm nodes are included in  $m$ . On average  $|\mathcal{D}^{\text{obs}}| = 196$  and  $|\mathcal{D}^{\text{int}}| = 123$  (500 ms discretisation). Model weights are never updated on either benchmark; we use PRIM-L throughout. The fine-tuned variant (PRIM-FT) trains with the encoder frozen on domain-matched simulator data: for PetShop the microservice simulator of Lohse et al. [26], for CausRCA a synthetic factory simulator with time as an additional feature [16] and multi-label cross-entropy loss. Details and hyperparameters are in Appendices B.4, C.

**PetShop** As shown in the Recall@3 in Table 1 Among methods that do not require a known causal graph, PRIM-FT achieves the highest average recall, outperforming all graph-not-given baselines except on the high-traffic scenarios, where heavy load introduces noise not captured by the prior or the fine-tuning simulator. On the low-availability and temporal-availability scenarios, PRIM-FT matches traversal and CIRCA, both of which require the causal graph, suggesting that when the prior models the problem well, the method can compensate for the absence of structural knowledge, even in a 44-node system.

**CausRCA** Based on the reported MAP@3 in Table 2 PRIM-FT is the best graph-not-given method on both the full and subsystem evaluations. On the coolant and hydraulics subsystems it is comparable

Table 1: Top-3 recall of the RCA methods for the PetShop data measuring the accuracy of including the correct root-cause node in the top-3 results. Results marked with \* are taken from Hardt et al. [13]; † denotes our methods. **Bold** indicates the best result per row overall; **blue** indicates the best result per row among graph-not-given methods.

traffic scenario	metric	graph given			graph not given				
		traversal*	circa*	counter-factual*	$\epsilon$ -diag.*	rcd*	corr*	PRIM†	PRIM FT†
low	latency	0.57	<b>0.86</b>	0.71	0.00	0.21	0.57	0.40	<b>0.60</b>
low	availability	<b>1.00</b>	<b>1.00</b>	0.42	0.00	0.75	0.92	<b>1.00</b>	<b>1.00</b>
high	latency	0.79	<b>1.00</b>	0.86	0.00	0.07	<b>0.79</b>	0.00	0.40
high	availability	<b>1.00</b>	0.00	0.00	0.33	0.00	<b>0.92</b>	0.25	0.25
temporal	latency	<b>1.00</b>	<b>1.00</b>	0.50	0.12	0.75	0.75	<b>0.83</b>	<b>0.83</b>
temporal	availability	<b>1.00</b>	<b>1.00</b>	0.25	0.12	0.75	0.75	0.83	<b>1.00</b>
average		<b>0.86</b>	0.81	0.46	0.10	0.39	<b>0.78</b>	0.50	0.65

to methods that have access to the causal graph, and on the subsystem mean it is only one decimal point below CausTR, a domain- and system-specific solution that uses the ground-truth graph. It is also better than the best CausTR algorithm using a graph obtained via causal discovery in the fine tuned version and only worse in coolant system for the base version.

Table 2: MAP@3 for RCA algorithms on the CausRCA benchmark. Results marked with \* are taken from Mehling et al. [29]; †Ours. **Bold** indicates best result per row overall; **blue** indicates best result per row among graph-not-given methods.

Dataset		graph given			graph not given					
		CausTR*	Rand Walk*	Page Rank*	Time Rank*	Baro*	Corr	CausTR +PC*	PRIM†	PRIM FT†
Coolant	Full	<b>0.99</b>	0.00	0.00	0.35	0.00	0.00	–	0.55	<b>0.63</b>
	Sub	<b>1.00</b>	0.14	<b>1.00</b>	0.85	0.88	0.15	0.87	0.75	<b>0.96</b>
Hydraulics	Full	<b>0.74</b>	0.00	0.11	0.18	0.26	0.13	–	0.61	<b>0.66</b>
	Sub	0.74	0.14	<b>0.98</b>	0.47	0.75	0.35	0.48	0.87	<b>0.91</b>
Probe	Full	<b>0.57</b>	0.00	0.00	<b>0.19</b>	0.00	0.00	–	0.00	0.00
	Sub	0.58	0.32	0.26	0.47	<b>0.63</b>	0.45	0.37	0.18	0.45
average	Full	<b>0.77</b>	0.00	0.04	0.24	0.09	0.05	–	0.39	<b>0.43</b>
	Sub	<b>0.78</b>	0.20	0.75	0.60	0.75	0.33	0.57	0.61	<b>0.77</b>

The full-system setting is harder: many sensors report constant values when no alarm is active, a regime not well represented in the base model’s prior; fine-tuning substantially narrows this gap. Performance on the probe subsystem remains low, likely due to its distinct fault signature. We additionally evaluated the baselines from the PetShop comparison (Appendix D.7), but their results are poor on CausRCA since most are designed for microservices or ignore temporal information; we omit them here for consistency with the evaluation setup of Mehling et al. [29].

## 7 Conclusion

In this paper we reformulate root cause analysis as a causal meta-learning problem and introduce PRIM, a model that identifies root causes via a single forward pass through a MACE transformer neural process. PRIM approximates a Bayesian model-averaged posterior over graph and functional mechanism uncertainty using synthetic priors, effectively performing a parameter-free Bayesian test at inference time without any statistical testing or model fitting on real data. PRIM is competitive with RCA baselines across diverse datasets and domains without requiring a causal graph or retraining at deployment time. Our synthetic experiments empirically confirm that  $\mathcal{D}^{\text{int}}$  and  $m$  can be jointly informative about  $T$ : PRIM recovers the true root cause with low error in three-node confounder and mediator topologies, multi-root-cause settings, and larger graphs. On the realistic benchmarks PetShop [13] and CausRCA [29], PRIM is competitive with both graph-free and graph-based RCA

methods when the prior captures the target system well. Our model adapts to new domains via lightweight finetuning on a domain-specific simulator, taking approximately three minutes on a GPU and yielding meaningful gains over the zero-shot baseline. Inference is equally practical, completing in approximately 17 ms on an A100 GPU, 35 ms on a laptop GPU, and 280 ms on CPU.

**Limitations** Our PRIM Method has several limitations. First, identifiability of  $T$  rests on the assumptions stated in Appendix A.2: an acyclic SCM, causal sufficiency, mechanism invariance for non-targets,  $\mathcal{I}$ -faithfulness, and the requirement that the observed anomaly is induced by the mechanism changes. Violations such as latent confounders or faithfulness violations compromise the theoretical guarantees. Second, a misspecified prior can degrade accuracy by failing to capture the true RCA distribution, as observed for the PetShop high-load and CausRCA Probe setups; both the model architecture and base prior construction leave room for refinement (e.g. following Dhir et al. [9]). Finally, PRIM cannot currently exploit a ground-truth graph when one is available.

## References

- [1] Matthew Ashman, Cristiana Diaconu, Junhyuck Kim, Lakee Sivaraya, Stratis Markou, James Requeima, Wessel P. Bruinsma, and Richard E. Turner. Translation equivariant transformer neural processes. In *Proceedings of the 41st International Conference on Machine Learning*, ICML'24, Vienna, Austria, 2024. JMLR.org.
- [2] Juan Carlos Belausteguigoitia. Causal chain analysis and root causes: the giwa approach. *AMBIO: A Journal of the Human Environment*, 33(1):7–12, 2004.
- [3] Kailash Budhathoki, Dominik Janzing, Patrick Bloebaum, and Hoiyi Ng. Why did the distribution change? In *International Conference on Artificial Intelligence and Statistics*, pages 1666–1674. PMLR, 2021.
- [4] Kailash Budhathoki, Lenon Minorics, Patrick Bloebaum, and Dominik Janzing. Causal structure-based root cause analysis of outliers. In Kamalika Chaudhuri, Stefanie Jegelka, Le Song, Csaba Szepesvari, Gang Niu, and Sivan Sabato, editors, *Proceedings of the 39th International Conference on Machine Learning*, volume 162 of *Proceedings of Machine Learning Research*, pages 2357–2369. PMLR, 17–23 Jul 2022. URL <https://proceedings.mlr.press/v162/budhathoki22a.html>.
- [5] Pengfei Chen, Yong Qi, Pengfei Zheng, and Di Hou. Causeinfer: Automatic and distributed performance diagnosis with hierarchical causality graph in large distributed systems. In *IEEE INFOCOM 2014-IEEE Conference on Computer Communications*, pages 1887–1895. IEEE, 2014.
- [6] Chris Cundy, Aditya Grover, and Stefano Ermon. Bcd nets: Scalable variational approaches for bayesian causal discovery. *Advances in Neural Information Processing Systems*, 34:7095–7110, 2021.
- [7] Anish Dhir, Matthew Ashman, James Requeima, and Mark van der Wilk. A meta-learning approach to bayesian causal discovery. In Y. Yue, A. Garg, N. Peng, F. Sha, and R. Yu, editors, *International Conference on Learning Representations*, volume 2025, pages 14158–14178, 2025. URL [https://proceedings.iclr.cc/paper\\_files/paper/2025/file/24faedc5853648d5857f2cf086a2acac-Paper-Conference.pdf](https://proceedings.iclr.cc/paper_files/paper/2025/file/24faedc5853648d5857f2cf086a2acac-Paper-Conference.pdf).
- [8] Anish Dhir, Cristiana Diaconu, Valentinian Mihai Lungu, James Requeima, Richard E. Turner, and Mark van der Wilk. Estimating interventional distributions with uncertain causal graphs through meta-learning. In *The Thirty-ninth Annual Conference on Neural Information Processing Systems*, 2025. URL <https://openreview.net/forum?id=Iqlcf40Ja>.
- [9] Anish Dhir, Ruby Sedgwick, Avinash Kori, Ben Glocker, and Mark van der Wilk. Continuous bayesian model selection for multivariate causal discovery. In *Forty-second International Conference on Machine Learning*, 2025. URL <https://openreview.net/forum?id=zydNWJzoVd>.
- [10] Frederick Eberhardt and Richard Scheines. Interventions and causal inference. *Philosophy of science*, 74(5):981–995, 2007.
- [11] Leo Feng, Hossein Hajimirsadeghi, Yoshua Bengio, and Mohamed Osama Ahmed. Latent bottlenecked attentive neural processes. In *The Eleventh International Conference on Learning Representations*, 2023. URL <https://openreview.net/forum?id=yIxtvizEA>.
- [12] Dan Geiger and David Heckerman. Parameter priors for directed acyclic graphical models and the characterization of several probability distributions. *The Annals of Statistics*, 30(5):1412–1440, October 2002. ISSN 0090-5364, 2168-8966. doi: 10.1214/aos/1035844981. URL <https://projecteuclid.org/journals/annals-of-statistics/volume-30/issue-5/Parameter-priors-for-directed-acyclic-graphical-models-and-the-characterization/10.1214/aos/1035844981.full>.
- [13] Michaela Hardt, William Roy Orchard, Patrick Blöbaum, Elke Kirschbaum, and Shiva Kasiswanathan. The petshop dataset — finding causes of performance issues across microservices. In Francesco Locatello and Vanessa Didelez, editors, *Proceedings of the Third Conference on*

- Causal Learning and Reasoning*, volume 236 of *Proceedings of Machine Learning Research*, pages 957–978. PMLR, 01–03 Apr 2024. URL <https://proceedings.mlr.press/v236/hardt24a.html>.
- [14] Noah Hollmann, Samuel Müller, Katharina Eggenberger, and Frank Hutter. TabPFN: A transformer that solves small tabular classification problems in a second. In *The Eleventh International Conference on Learning Representations*, 2023.
- [15] Noah Hollmann, Samuel Müller, Lennart Purucker, Arjun Krishnakumar, Max Körfer, Shi Bin Hoo, Robin Tibor Schirrmeyer, and Frank Hutter. Accurate predictions on small data with a tabular foundation model. *Nature*, 637(8045):319–326, January 2025. ISSN 1476-4687. doi: 10.1038/s41586-024-08328-6. URL <https://www.nature.com/articles/s41586-024-08328-6>.
- [16] Shi Bin Hoo, Samuel Müller, David Salinas, and Frank Hutter. From tables to time: Extending tabPFN-v2 to time series forecasting. *arXiv preprint arXiv:2501.02945*, 2025.
- [17] Azam Ikram, Sarthak Chakraborty, Subrata Mitra, Shiv Saini, Saurabh Bagchi, and Murat Kocaoglu. Root cause analysis of failures in microservices through causal discovery. *Advances in Neural Information Processing Systems*, 35:31158–31170, 2022.
- [18] Azam Ikram, Kenneth Lee, Shubham Agarwal, Shiv Kumar Saini, Saurabh Bagchi, and Murat Kocaoglu. Root cause analysis of failures from partial causal structures. In *The 41st Conference on Uncertainty in Artificial Intelligence*, 2025. URL <https://openreview.net/forum?id=5He0DZrG9E>.
- [19] Amin Jaber, Murat Kocaoglu, Karthikeyan Shanmugam, and Elias Bareinboim. Causal Discovery from Soft Interventions with Unknown Targets: Characterization and Learning. In *Advances in Neural Information Processing Systems*, volume 33, pages 9551–9561. Curran Associates, Inc., 2020. URL <https://papers.nips.cc/paper/2020/hash/6cd9313ed34ef58bad3fdd504355e72c-Abstract.html>.
- [20] Abhishek Jayswal, Xiang Li, Anand Zanwar, Helen H Lou, and Yinlun Huang. A sustainability root cause analysis methodology and its application. *Computers & chemical engineering*, 35(12):2786–2798, 2011.
- [21] Jinzhou Li, Benjamin B Chu, Ines F Scheller, Julien Gagneur, and Marloes H Maathuis. Root cause discovery via permutations and cholesky decomposition. *Journal of the Royal Statistical Society Series B: Statistical Methodology*, page qkaf066, 2025.
- [22] Mingjie Li, Zeyan Li, Kanglin Yin, Xiaohui Nie, Wenchi Zhang, Kaixin Sui, and Dan Pei. Causal inference-based root cause analysis for online service systems with intervention recognition. In *Proceedings of the 28th ACM SIGKDD Conference on Knowledge Discovery and Data Mining*, KDD ’22, page 3230–3240, New York, NY, USA, 2022. Association for Computing Machinery. ISBN 9781450393850. doi: 10.1145/3534678.3539041. URL <https://doi.org/10.1145/3534678.3539041>.
- [23] Shuai Liang, Pengfei Chen, Bozhe Tian, Gou Tan, Maohong Xu, Youjun Qu, Yahui Zhao, Yiduo Shang, and Chongkang Tan. MetaRCA: A Generalizable Root Cause Analysis Framework for Cloud-Native Systems Powered by Meta Causal Knowledge, March 2026. URL <http://arxiv.org/abs/2603.02032>. arXiv:2603.02032 [cs].
- [24] JinJin Lin, Pengfei Chen, and Zibin Zheng. Microscope: Pinpoint performance issues with causal graphs in micro-service environments. In *International Conference on Service-Oriented Computing*, pages 3–20. Springer, 2018.
- [25] Dewei Liu, Chuan He, Xin Peng, Fan Lin, Chenxi Zhang, Shengfang Gong, Ziang Li, Jiayu Ou, and Zheshun Wu. Microhecl: High-efficient root cause localization in large-scale microservice systems. In *2021 IEEE/ACM 43rd International Conference on Software Engineering: Software Engineering in Practice (ICSE-SEIP)*, pages 338–347. IEEE, 2021.
- [26] Christopher Lohse, Adrian Selk, Amadou Ba, Jonas Wahl, and Marco Ruffini. Licence to scale: A microservice simulation environment for benchmarking agentic ai. Accepted at NeurIPS 2025 Workshop Scaling Environments for Agents (SEA), December 2025.

- [27] Lars Lorch, Jonas Rothfuss, Bernhard Schölkopf, and Andreas Krause. Dibs: Differentiable bayesian structure learning. *Advances in Neural Information Processing Systems*, 34:24111–24123, 2021.
- [28] Lawrence A Lynn and J Paul Curry. Patterns of unexpected in-hospital deaths: a root cause analysis. *Patient safety in surgery*, 5(1):3, 2011.
- [29] Carl Willy Mehling, Sven Pieper, Tobias Lüke, Julius Döbelt, and Steffen Ihlenfeldt. Enabling Joint Benchmarking of Automated Root Cause Analysis and Causal Discovery in Manufacturing Using the *causRCA* Dataset. *Procedia CIRP*, 139:114–120, January 2026. ISSN 2212-8271. doi: 10.1016/j.procir.2025.09.010. URL <https://www.sciencedirect.com/science/article/pii/S221282712500976X>.
- [30] Samuel Müller, Noah Hollmann, Sebastian Pineda Arango, Josif Grabocka, and Frank Hutter. Transformers can do bayesian inference. In *International Conference on Learning Representations*, 2022. URL <https://openreview.net/forum?id=KSugKcbNf9>.
- [31] Tung Nguyen and Aditya Grover. Transformer neural processes: Uncertainty-aware meta learning via sequence modeling. *ArXiv*, abs/2207.04179, 2022. URL <https://api.semanticscholar.org/CorpusID:250340974>.
- [32] William Roy Orchard, Nastaran Okati, Sergio Hernan Garrido Mejia, Patrick Blöbaum, and Dominik Janzing. Root cause analysis of outliers with missing structural knowledge. In *The Thirty-ninth Annual Conference on Neural Information Processing Systems*, 2026. URL <https://openreview.net/forum?id=7Nxq4RQApu>.
- [33] Lawrence Page, Sergey Brin, Rajeev Motwani, and Terry Winograd. The pagerank citation ranking: Bringing order to the web. Technical report, Stanford infolab, 1999.
- [34] Judea Pearl. Causal diagrams for empirical research. *Biometrika*, 82(4):669–688, 1995.
- [35] Judea Pearl. *Causality*. Cambridge university press, 2009.
- [36] Luan Pham, Huong Ha, and Hongyu Zhang. Baro: Robust root cause analysis for microservices via multivariate bayesian online change point detection. *Proceedings of the ACM on Software Engineering*, 1(FSE):2214–2237, July 2024. ISSN 2994-970X. doi: 10.1145/3660805.
- [37] Jake Robertson, Arik Reuter, Siyuan Guo, Noah Hollmann, Frank Hutter, and Bernhard Schölkopf. Do-PFN: In-context learning for causal effect estimation. In *The Thirty-ninth Annual Conference on Neural Information Processing Systems*, 2026. URL <https://openreview.net/forum?id=0aNb19b56B>.
- [38] Daniela Schkoda and Dominik Janzing. Root cause analysis of outliers in unknown cyclic graphs. *arXiv preprint arXiv:2510.06995*, 2025.
- [39] Suganya Selvaraj and Shanmughavel Piramanayagam. Impact of gene mutation in the development of parkinson’s disease. *Genes & diseases*, 6(2):120–128, 2019.
- [40] Huasong Shan, Yuan Chen, Haifeng Liu, Yunpeng Zhang, Xiao Xiao, Xiaofeng He, Min Li, and Wei Ding.  $\epsilon$ -diagnosis: Unsupervised and real-time diagnosis of small-window long-tail latency in large-scale microservice platforms. In *The World Wide Web Conference, WWW ’19*, page 3215–3222, New York, NY, USA, 2019. Association for Computing Machinery. ISBN 9781450366748. doi: 10.1145/3308558.3313653. URL <https://doi.org/10.1145/3308558.3313653>.
- [41] Jacopo Soldani and Antonio Brogi. Anomaly detection and failure root cause analysis in (micro) service-based cloud applications: A survey. *ACM Comput. Surv.*, 55(3), February 2022. ISSN 0360-0300. doi: 10.1145/3501297. URL <https://doi.org/10.1145/3501297>.
- [42] Peter Spirtes and Kun Zhang. Causal discovery and inference: concepts and recent methodological advances. In *Applied informatics*, volume 3, pages 1–28. Springer, 2016.
- [43] Peter Spirtes, Clark N Glymour, and Richard Scheines. *Causation, prediction, and search*. MIT press, 2000.

- [44] Chandler Squires, Yuhao Wang, and Caroline Uhler. Permutation-based causal structure learning with unknown intervention targets. In *Conference on Uncertainty in Artificial Intelligence*, pages 1039–1048. PMLR, 2020.
- [45] Burak Varici, Karthikeyan Shanmugam, Prasanna Sattigeri, and Ali Tajer. Scalable intervention target estimation in linear models. In M. Ranzato, A. Beygelzimer, Y. Dauphin, P.S. Liang, and J. Wortman Vaughan, editors, *Advances in Neural Information Processing Systems*, volume 34, pages 1494–1505. Curran Associates, Inc., 2021. URL [https://proceedings.neurips.cc/paper\\_files/paper/2021/file/0b94ce08688c6389ce7b68c52ce3f8c7-Paper.pdf](https://proceedings.neurips.cc/paper_files/paper/2021/file/0b94ce08688c6389ce7b68c52ce3f8c7-Paper.pdf).
- [46] Burak Varici, Karthikeyan Shanmugam, Prasanna Sattigeri, and Ali Tajer. Intervention target estimation in the presence of latent variables. In James Cussens and Kun Zhang, editors, *Proceedings of the Thirty-Eighth Conference on Uncertainty in Artificial Intelligence*, volume 180 of *Proceedings of Machine Learning Research*, pages 2013–2023. PMLR, 01–05 Aug 2022. URL <https://proceedings.mlr.press/v180/varici22a.html>.
- [47] Ashish Vaswani, Noam Shazeer, Niki Parmar, Jakob Uszkoreit, Llion Jones, Aidan N Gomez, Łukasz Kaiser, and Illia Polosukhin. Attention is all you need. *Advances in neural information processing systems*, 30, 2017.
- [48] Karren Yang, Abigail Katcoff, and Caroline Uhler. Characterizing and learning equivalence classes of causal dags under interventions. In *International Conference on Machine Learning*, pages 5541–5550. PMLR, 2018.
- [49] Yuqin Yang, Saber Salehkaleybar, and Negar Kiyavash. Learning unknown intervention targets in structural causal models from heterogeneous data. In Sanjoy Dasgupta, Stephan Mandt, and Yingzhen Li, editors, *Proceedings of The 27th International Conference on Artificial Intelligence and Statistics*, volume 238 of *Proceedings of Machine Learning Research*, pages 3187–3195. PMLR, 02–04 May 2024. URL <https://proceedings.mlr.press/v238/yang24d.html>.

## A Derivations and Identifiability of Root Causes

### A.1 Derivation of the Bayesian Posterior

Since the components of  $\mathbf{f} \equiv (\mathbf{f}^{\text{obs}}, \mathbf{f}^{\text{int}})$  are not independent, we for convenience do not model both functions separately in the posterior. The full distribution we want to estimate is:

$$p(T, \mathbf{f}, \mathcal{G} | \mathcal{D}^{\text{obs}}, \mathcal{D}^{\text{int}}, m) \quad (\text{A.1})$$

by marginalising out  $\mathcal{G}$  we get

$$p(T, \mathbf{f} | \mathcal{D}^{\text{obs}}, \mathcal{D}^{\text{int}}, m) = \sum_{\mathcal{G}} p(T, \mathbf{f}, \mathcal{G} | \mathcal{D}^{\text{obs}}, \mathcal{D}^{\text{int}}, m) \quad (\text{A.2})$$

by additionally marginalising out  $\mathbf{f}$  we get

$$p(T | \mathcal{D}^{\text{obs}}, \mathcal{D}^{\text{int}}, m) = \int \left( \sum_{\mathcal{G}} p(T, \mathbf{f}, \mathcal{G} | \mathcal{D}^{\text{obs}}, \mathcal{D}^{\text{int}}, m) \right) d\mathbf{f} \quad (\text{A.3})$$

which we can rewrite using the chain rule to

$$\sum_{\mathcal{G}} \int p(T | \mathbf{f}, \mathcal{G}, \mathcal{D}^{\text{obs}}, \mathcal{D}^{\text{int}}, m) p(\mathbf{f} | \mathcal{G}, \mathcal{D}^{\text{obs}}, \mathcal{D}^{\text{int}}, m) p(\mathcal{G} | \mathcal{D}^{\text{obs}}, \mathcal{D}^{\text{int}}, m) d\mathbf{f} \quad (\text{A.4})$$

The factorization of the distribution of the Bayesian Model gives the the following conditional independence statements  $T \perp \mathcal{D}^{\text{obs}}, \mathcal{D}^{\text{int}} | \mathbf{f}, m, \mathcal{G}$  meaning: if we know the function difference, the graph, and the observed anomaly, this is sufficient to find the root cause without observational and interventional data. Further  $\mathcal{G} \perp m | \mathcal{D}^{\text{obs}}, \mathcal{D}^{\text{int}}$  meaning: the graph is determined by the data alone and the anomaly carries no additional information about it. Likewise, we get  $\mathbf{f} \perp m | \mathcal{G}, \mathcal{D}^{\text{obs}}, \mathcal{D}^{\text{int}}$  meaning: the function difference is identified from the data and the graph, and where the anomaly was observed carries no additional information about it. We can therefore rewrite this as

$$p(T | \mathcal{D}^{\text{obs}}, \mathcal{D}^{\text{int}}, m) = \sum_{\mathcal{G}} \int p(T | \mathbf{f}, \mathcal{G}, m) p(\mathbf{f} | \mathcal{G}, \mathcal{D}^{\text{obs}}, \mathcal{D}^{\text{int}}) p(\mathcal{G} | \mathcal{D}^{\text{obs}}, \mathcal{D}^{\text{int}}) d\mathbf{f} \quad (\text{A.5})$$

## A.2 Identifiability of the Root Cause(s)

Here we provide our reasoning for why the posterior  $p(T \mid \mathcal{D}^{\text{obs}}, \mathcal{D}^{\text{int}}, m)$  concentrates on the correct  $T$  in the infinite-data limit. The argument is fully nonparametric and covers both soft and hard interventions. We focus on the multi-sample interventional setting, in which each interventional regime provides enough samples to identify its conditional distributions; this covers all our experiments except the single-anomaly CausRCA case. The argument relies on the identifiability result of Squires et al. [44].

**Setting** We consider  $K \geq 1$  interventional regimes. For each regime  $k$ , let  $T_{\text{full}}^k$  denote the set of nodes whose mechanism is altered in regime  $k$  relative to the observational regime, and write  $T_{\text{full}} = \bigcup_{k=1}^K T_{\text{full}}^k$  for the union of all mechanism-changed nodes across regimes. The root cause set  $T \subseteq T_{\text{full}}$  is the subset of mechanism-changed nodes that are causally responsible for the observed anomaly  $m$ , as defined in the main text.

**Definition A.1** ( $\mathcal{I}$ -Markov equivalence [48; 44]). Two pairs of DAG and intervention target list,  $(\mathcal{G}_1, T_{\text{full},1})$  and  $(\mathcal{G}_2, T_{\text{full},2})$ , are  $\mathcal{I}$ -Markov equivalent if they induce the same set of observational and interventional distributions over  $X$ , where each interventional regime preserves the conditional  $p(X_i \mid \text{pa}_{\mathcal{G}}(i))$  for non-intervened nodes. The equivalence class of  $(\mathcal{G}, T_{\text{full}})$  under this relation is the  $\mathcal{I}$ -Markov equivalence class ( $\mathcal{I}$ -MEC).

**Assumption A.1** (Acyclic SCM). The data  $\mathcal{D}^{\text{obs}}$  and  $\mathcal{D}^{\text{int}} = \{\mathcal{D}^{\text{int},k}\}_{k=1}^K$  are generated by a structural causal model whose causal graph  $\mathcal{G}$  is a directed acyclic graph over the observed variables  $X = (X_1, \dots, X_n)$ .

**Assumption A.2** (Causal sufficiency). There are no latent confounders.

**Assumption A.3** (Mechanism invariance for non-targets). For each interventional regime  $k$  and each  $X_i \notin T_{\text{full}}^k$ , the conditional  $p(X_i \mid \text{pa}_{\mathcal{G}}(i))$  is invariant between the observational regime and regime  $k$ . Both soft and hard interventions on the targets in  $T_{\text{full}}^k$  are permitted.

**Assumption A.4** ( $\mathcal{I}$ -faithfulness; Squires et al. [44], Assumption 2). The observational distribution is faithful to  $\mathcal{G}$  in the usual sense, and conditional invariances across regimes correspond exactly to  $d$ -separations between intervention nodes and observed variables in the *augmented graph*  $\mathcal{G}^{\mathcal{I}}$  (the graph obtained from  $\mathcal{G}$  by adding, for each regime  $k$ , an intervention node  $\zeta_k$  with edges  $\zeta_k \rightarrow X_i$  for every  $X_i \in T_{\text{full}}^k$ ). Intuitively, this rules out interventions that leave no statistical trace: every genuine mechanism change must produce a detectable difference in some conditional distribution, and effects from distinct interventions or distinct paths must not cancel exactly.

**Assumption A.5** (Anomaly variable). The observed anomaly  $m$  corresponds to a variable in  $X$  whose anomalous behaviour is induced (directly or indirectly) by mechanism changes at a subset  $T \subseteq T_{\text{full}}$  of intervened nodes. We refer to  $T$  as the *root cause set*.

### Identifiability of the Root Causes

We first invoke the identifiability result of Squires et al. [44]. Their Assumption 2 (our Assumption A.4) states that for any regime  $k$  and any disjoint  $A, C$ ,

$$(A \perp\!\!\!\perp \zeta_k \mid C \cup \zeta_{[K] \setminus \{k\}})_{\mathcal{G}^{\mathcal{I}}} \iff f^k(x_A \mid x_C) = f^{\text{obs}}(x_A \mid x_C).$$

The forward direction is the  $\mathcal{I}$ -Markov property (Assumptions A.1, A.2); the reverse is faithfulness (Assumption A.4), which rules out coincidental cancellations that would mask a genuine intervention.

Applying this with  $A = \{i\}$  identifies the intervention targets, as in Squires et al. [44, §3.2]. A node  $i$  lies in  $T_{\text{full}}^k$  iff  $\zeta_k$  and  $i$  are adjacent in  $\mathcal{G}^{\mathcal{I}}$ , and adjacent nodes cannot be  $d$ -separated by any conditioning set. The biconditional above (Assumption A.4) translates this into the data-determined statement that no  $C$  makes  $f^k(x_i \mid x_C)$  and  $f^{\text{obs}}(x_i \mid x_C)$  agree; for non-targets, conditioning on  $\text{pa}_{\mathcal{G}}(i)$  does, by mechanism invariance (Assumption A.3). Hence  $T_{\text{full}}^k$ , and so  $T_{\text{full}} := \bigcup_k T_{\text{full}}^k$ , is identifiable, for both soft and hard interventions (Assumption A.3).

The set  $T_{\text{full}}$  contains every node whose mechanism has changed in any regime, regardless of whether that change is causally relevant to the observed anomaly. Conditioning on  $m$  is what distinguishes *root cause analysis* from intervention target estimation: a node  $i \in T_{\text{full}}$  can only have contributed to the anomaly at  $m$  if it lies upstream of  $m$  in the causal graph (Assumption A.5). Mechanism changes

at nodes that are not ancestors of  $m$  propagate nothing to  $m$  and are therefore irrelevant to the root cause analysis, even though they are genuine interventions. The root cause set is thus

$$T = \{i \in T_{\text{full}} : i \in \text{An}_{\mathcal{G}}(m)\}.$$

The same biconditional (Assumption A.4), applied with  $A = \{m\}$ , identifies  $T$ . Under causal sufficiency (Assumption A.2),  $\zeta_k$  is d-connected to  $m$  exactly when some target in  $T_{\text{full}}^k$  is an ancestor of  $m$  in  $\mathcal{G}$  (Assumption A.1), so a node in  $T_{\text{full}}$  is an ancestor of  $m$  iff no conditioning set makes the interventional and observational distributions of  $m$  agree, a pattern determined by the data alone. Every DAG in the  $\mathcal{I}$ -MEC must therefore agree on which nodes in  $T_{\text{full}}$  are ancestors of  $m$ , even if it disagrees about the rest of the ancestor relation. Marginalising over the  $\mathcal{I}$ -MEC yields the correct  $T$  in the infinite-data limit, and residual ambiguities among nodes outside  $T_{\text{full}}$  do not affect  $T$ .

**Compatibility of the prior with the assumptions.** Our prior generation fulfils these assumptions by design: we sample only DAGs (no cycles) with no latent confounders, satisfying Assumptions A.1 and A.2. Soft interventions are modelled so as not to alter the graph structure, and hard interventions only drop the parents of the target node (more details in Appendix B.1); in both cases the conditionals of non-target nodes are unchanged, satisfying Assumption A.3. Because mechanism parameters are drawn from continuous distributions, the probability that an intervention is exactly cancelled by another intervention or by the functional form of a downstream mechanism is zero (a standard generic-position argument), so Assumption A.4 holds almost surely. Access to the anomaly variable is standard in RCA evaluations and is provided by our prior generation, satisfying Assumption A.5. Thus both the prior generation and the synthetic evaluation setups satisfy all the assumptions used above.

## B Data and Prior Design

### B.1 Data Generation

The data generation process is illustrated in Figure 5. For each training instance, a DAG  $\mathcal{G}$  and a set of structural equations  $\mathbf{f}$  are sampled to form an SCM, with mechanisms drawn from linear, tanh, MLP, or GP families and a shared noise distribution across nodes.

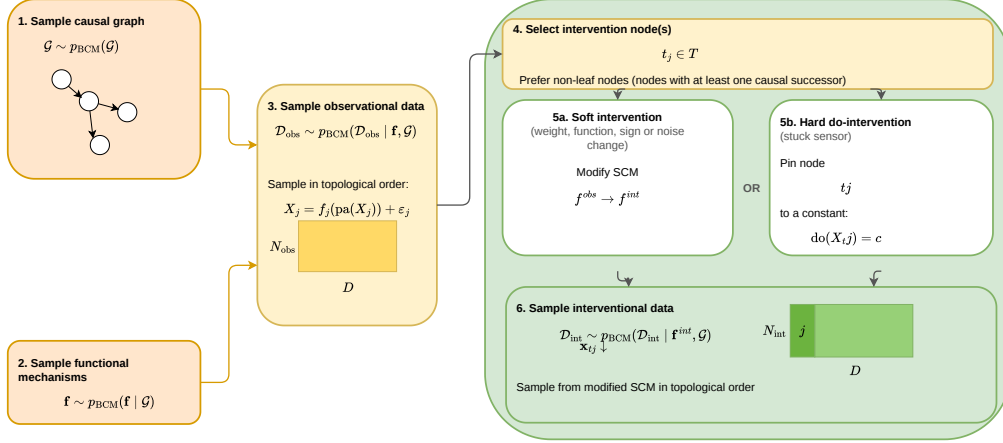


Figure 5: Overview of the data generation process. A causal graph  $\mathcal{G}$  and functional mechanisms  $\mathbf{f}$  are sampled to define an SCM. Observational data  $\mathcal{D}_{\text{obs}}$  is drawn by ancestral sampling, after which a target node  $t_j \in T$  is selected and the SCM is perturbed via a soft intervention ( $\mathbf{f}^{\text{obs}} \rightarrow \mathbf{f}^{\text{int}}$ ) or a hard do-intervention pinning  $t_j$  to a constant. Interventional data  $\mathcal{D}_{\text{int}}$  is then sampled from the modified SCM.

Observational data  $\mathcal{D}_{\text{obs}} \in \mathbb{R}^{N_{\text{obs}} \times D}$  is collected by forward-sampling in topological order. Root-cause nodes  $T$  are then selected and a soft or hard intervention is applied, yielding interventional data  $\mathcal{D}_{\text{int}} \in \mathbb{R}^{N_{\text{int}} \times D}$ . The triple  $(\mathcal{D}_{\text{obs}}, \mathcal{D}_{\text{int}}, T)$  forms one training example. Note for all experiments except the finetuning for multiRCA and CausRCA  $|T| = 1$  meaning we only inject one root cause.

### B.2 Prior over Causal Models

The prior design follows the design of Dhir et al. [7] with some specific changes to make it more suitable for the root cause analysis tasks such as different types of interventions, constant baselines and a rich range of noise distributions as well as only sampling sparse graphs. The tree model sizes are trained: small ( $K_{\text{min}} = 2, K_{\text{max}} = 5$ ), medium ( $K_{\text{min}} = 2, K_{\text{max}} = 10$ ), and large ( $K_{\text{min}} = 17, K_{\text{max}} = 100$ ).

**Graph structure** As the usual set-up for root cause analysis rarely includes dense causal graph we assume a sparse structure of the causal DAG. Each episode samples a DAG  $\mathcal{G}$  over  $K \sim \text{Unif}(K_{\text{min}}, K_{\text{max}})$  nodes. The graph family is chosen uniformly from Erdős–Rényi (ER), Barabási–Albert (BA), and bipartite. Edge density is controlled via expected in-degree  $\bar{d} \sim \text{Unif}(1.8, 2.5)$ , giving  $p_{\text{edge}} = \bar{d}/(K-1)$ . A uniform node-index permutation removes topological-ordering bias.

**Structural equations** An episode draws one mechanism family uniformly from {linear, tanh, NN, GP, baseline} and applies it to all nodes.

**Linear.**  $X_k = \mathbf{w}_k^\top \tilde{X}_{\text{pa}(k)} + \lambda_k h_k + \eta_k \varepsilon_k$ , where  $\tilde{X}_{\text{pa}(k)}$  are parent values z-scored column-wise,  $w_{ki} \sim \mathcal{N}(0, 3)$ ,  $h_k \sim \mathcal{N}(0, 1)$  is a latent confounder with weight  $\lambda_k \sim \mathcal{N}(0, 1)$ , and  $\eta_k \sim \text{Gamma}(2.5, 2.5)$  provides heteroscedastic noise.

**Tanh**  $X_k = \mathbf{w}_k^\top \tanh(S_k \odot X_{\text{pa}(k)}) + \lambda_k h_k + \varepsilon_k$ , with  $w_{ki} \sim \mathcal{N}(0, 3)$  and  $s_{ki} \sim \text{Unif}(0.8, 1.5)$ .

### Neural network

$$X_k = \begin{cases} \text{NN}_k(\varepsilon_k) & \text{pa}(k) = \emptyset \\ \text{NN}_k(X_{\text{pa}(k)}) + \varepsilon_k & \text{otherwise} \end{cases} \quad (\text{B.1})$$

Each  $\text{NN}_k$  is a randomly initialised MLP; per-layer activations are sampled from  $\{\sigma, \tanh, \text{ReLU}\}$ .

**Gaussian process** The kernel is chosen uniformly from  $\{\text{RBF}, \text{Matérn-1/2}, \text{Matérn-3/2}\}$  with lengthscale  $\ell \sim \log\text{-Unif}(0.1, 5.0)$ , output scale  $\alpha \sim \text{Unif}(0.5, 2.0)$ , and observation noise variance  $\sim \text{Gamma}(2.5, 0.4)$ . A  $\mathcal{N}(0, 1)$  latent variable is appended to parent inputs to model unobserved confounders.

**Constant-baseline** Mimics failure metrics: each node operates near  $b \sim \text{Unif}(90, 100)$  with near-zero noise, so faults produce z-scores that saturate the  $\pm 10$  clipping boundary.

**Exogenous noise** Each SCM draws its noise distribution uniformly from  $\{\text{Gaussian}, \text{Poisson}, \text{salt-and-pepper}, \text{truncated-exponential}\}$  with scale  $\sigma \sim \log\text{-Unif}(0.05, 2.0)$ .

**Interventions** A non-leaf node  $T$  is intervened on using one of three mechanisms: weight-change (80%), additive shift (15%), or hard do-intervention (5%).

**Weight change** For linear/nonlinear SCMs, incoming weights at  $T$  are rescaled and sign-randomised:  $\tilde{w}_{Ti} = c \cdot s_i \cdot w_{Ti}$ ,  $s_i \sim \text{Unif}\{-1, +1\}$ ,  $c \sim \text{Unif}(3.0, 5.0)$ . For NN SCMs, either all layer weights are scaled by  $c$  (with random sign flips) or each activation is replaced by a different function from  $\{\sigma, \tanh, \text{ReLU}\}$ , chosen with equal probability. Root nodes are intervened on by scaling the noise standard deviation by  $c$ .

**Additive shift** A constant offset  $\delta = \pm \text{Unif}(0.5, 2.0) \cdot \sigma \cdot c$  is added to  $T$ 's output and propagates through its descendants. For constant-baseline SCMs,  $\delta = -b \cdot \text{Unif}(0.03, 0.15)$ .

**Hard do-intervention.** Node  $T$  is pinned to a constant 2–4 standard deviations from its observational mean (“stuck sensor”), collapsing its variance to zero.

### B.3 Padding and Variable Graph Size

PRIM operates on graphs of varying size  $k \leq K_{\max}$ , where  $K_{\max}$  is the maximum number of nodes the model was trained on. To handle variable-size inputs with a fixed-size transformer, we follow the padding strategy of Hollmann et al. [14, 15].

**Data padding** For a graph with  $k$  real nodes, both  $\mathcal{D}^{\text{obs}}$  and  $\mathcal{D}^{\text{int}}$  are zero-padded along the node dimension to size  $K_{\max}$ . Real node values are z-score normalised and then scaled by a factor of  $K_{\max}/k$  before padding, so that the magnitude of activations remains consistent regardless of graph size. Padded positions are filled with zero.

**Attention masking** A binary padding mask is constructed such that positions  $j \geq k$  are marked as padding. This mask is passed to all MACE transformer layers, where it is used as a key padding mask in the node-level attention step, preventing padded positions from contributing to attention scores. After every LayerNorm operation, padded positions are explicitly re-zeroed by elementwise multiplication with the mask, preventing LayerNorm from reintroducing non-zero values at padding locations.

**Output masking** At inference time, logits at padding positions  $j \geq k$  are set to  $-\infty$  before the softmax, ensuring the model can only predict valid nodes as root causes. During training, the same masking is applied before the cross-entropy loss.

### B.4 Simulator for Finetuning PetShop

The finetuning data is drawn from the microservice simulator created by Lohse et al. [26], which generates latency traces for randomised service dependency graphs with 3–15 nodes across three traffic regimes (low, medium, high). The dataset comprises 200 environments, each containing one normal-operation recording (300 timesteps) and three anomaly scenarios corresponding to faults of type *cpu\_leak*, *memory\_leak*, or *degradation* injected at different services, yielding 600 labelled fault

cases in total. The normal latency window (60 timesteps) serves as the observational data  $D_{\text{obs}}$  and the post-injection window (5 timesteps) as the interventional data  $D_{\text{int}}$ , both z-score normalised using the normal-data statistics and zero-padded to the model’s maximum node dimension. The decoder is updated during a single pass over all 600 fault cases with learning rate  $10^{-4}$ , while the backbone encoder remains frozen.

### B.5 Prior for Finetuning CausRCA

We generate synthetic training data following the causal structure of event-driven industrial systems [29]. For each environment we sample a random DAG  $\mathcal{G} = (\mathcal{V}, \mathcal{E})$  over  $K \in [25, 40]$  nodes (probe), [12, 18] (coolant), or [14, 20] (hydraulics), drawn from Erdős–Rényi or Barabási–Albert random graph models with edge probability  $p \sim \mathcal{U}(0.2, 0.5)$ . This is to mimic the CausRCA system without explicitly training on data from it.

**Normal regime** Continuous nodes follow a mean-reverting auto regressive process:

$$x_i(t) = \mu_i + 0.95 \cdot (x_i(t-1) - \mu_i) + \varepsilon_i(t), \quad \varepsilon_i \sim \mathcal{N}(0, \sigma_i^2). \quad (\text{B.2})$$

Binary nodes are constant at their baseline  $\mu_i \in \{0, 1\}$  with small Gaussian noise  $\sigma_i = 0.005$ .

**Fault injection** Each scenario involves  $|T| \in \{1, 2, 3\}$  simultaneous, independent root causes (sampled with probabilities 0.70/0.20/0.10), reflecting the multi-fault conditions reported in the original dataset. For each node  $i$ , let  $d_i = \min_{r \in T} \text{dist}(r, i)$  be the shortest DAG hop distance from any root cause. The fault propagates with delay  $\delta_i = d_i \cdot \tau$ , where  $\tau \sim \mathcal{U}(\tau_{\min}, \tau_{\max})$  steps per hop. The faulty signal is:

$$x_i^{\text{fault}}(t) = \begin{cases} \mu_i + m_i \cdot \alpha^{d_i} + \varepsilon_i(t) & t \geq \delta_i, \\ \mu_i + \varepsilon_i(t) & t < \delta_i, \end{cases} \quad (\text{B.3})$$

where  $m_i = \sigma_i \cdot 15$  (clipped to  $\pm 10$  after z-normalisation) is the fault magnitude and  $\alpha = 0.30$  is the attenuation per hop. Binary descendants flip state with probability  $0.75^{d_i}$  at step  $\delta_i$ . Nodes not reachable from  $T$  remain at baseline.

**Preprocessing** All signals are z-normalised using pre-fault statistics and clipped to  $[-10, 10]$ , then scaled by  $K_{\text{max}}/K$  to fill the model’s  $K_{\text{max}}$ -dimensional input space. A *time-as-feature* node [16] is appended at position  $K+1$ , holding a linear ramp

$$\ell(t) = \frac{K_{\text{max}}}{K} \cdot \left( \frac{2t}{T_{\text{max}} - 1} - 1 \right), \quad (\text{B.4})$$

where  $T_{\text{max}}$  is the number of time steps in the scenario. The ramp has zero mean, so that  $\bar{\ell}^{\text{int}} - \bar{\ell}^{\text{obs}} \approx 0$  and the node does not bias output logits. It is visible to all transformer attention layers, providing a temporal coordinate that allows the model to distinguish nodes that changed early (root causes) from nodes that changed later (downstream alarms).

**Full-mode environments** To cover the full-graph evaluation setting ( $K_{\text{max}} = 92$  nodes), we embed one sub-environment’s  $K_{\text{sub}}$  active nodes at randomly shuffled positions within a 92-slot grid, leaving the remaining  $92 - K_{\text{sub}}$  positions at zero — matching the constant signals from uninvolved subsystems.

**Loss** The ground-truth label is a multi-hot vector  $\mathbf{y} \in \{0, 1\}^{K_{\text{max}}}$  with a 1 for each active root cause. We minimise cross-entropy independently for each positive entry in  $\mathbf{y}$ , plus an alarm-avoidance penalty  $\lambda \cdot \text{softplus}(\hat{y}_{\text{alarm}})$  with  $\lambda = 0.40$  to prevent the model from exploiting the alarm node as a shortcut:

$$\mathcal{L} = \frac{1}{|T|} \sum_{r \in T} \ell_{\text{CE}}(\hat{\mathbf{y}}, r) + \lambda \cdot \text{softplus}(\hat{y}_{\text{alarm}}), \quad (\text{B.5})$$

where  $\ell_{\text{CE}}(\hat{\mathbf{y}}, r) = -\log \hat{y}_r$  is the per-target cross-entropy.

Each epoch iterates over all  $200 \times 8 = 1,600$  (environment, scenario) pairs, each yielding one gradient step on 4 query samples, for a total of 1,600 gradient steps per epoch across 5 epochs.

## C Hyperparameters and Compute

All models use embedding dimension  $d = 160$ ,  $L = 8$  MACE layers, 8 attention heads, MLP hidden size 512, and dropout 0.1. The small and medium models are trained on 80,000 unique samples from 20,000 distinct SCMs; the large model on 1,920,000 samples from 480,000 distinct SCMs. Hyperparameters for all training and finetuning runs are listed in Table A.1; compute requirements are summarised in Table A.3; the model used per experiment is given in Table A.2.

Table A.1: Hyperparameters for training and finetuning.

Component	Hyperparameter	Value
Training (all models)	Optimizer	AdamW
	Learning rate	$5 \times 10^{-4}$
	Weight decay	0.01
	Episodes / epoch	1,000
	Queries / episode ( $n_q$ )	4
	$n_{\text{obs}}$	Unif(5, 500)
	$n_{\text{int}}$	Unif(1, 200)
Training (per model)	Dropout	0.1
	Small ( $K_{\min} = 2$ , $K_{\max} = 5$ ), 40 epochs	4×A100-80GB
	Medium ( $K_{\min} = 2$ , $K_{\max} = 10$ ), 40 epochs	4×A100-80GB
	Large ( $K_{\min} = 17$ , $K_{\max} = 100$ ), 60 epochs	8×A100-80GB
PetShop FT	Learning rate	$1 \times 10^{-4}$
	Epochs	1
	$n_{\text{obs}}$	60
	$n_{\text{int}}$	5
CausRCA FT	Learning rate	$3 \times 10^{-5}$
	Epochs	4
	Warmup	5% of steps
Multi-RC FT	Learning rate	$3 \times 10^{-5}$
	Epochs	5
	$n_{\text{obs}}$	Unif(40, 150)
	$n_{\text{int}}$	Unif(5, 20)
Ablation FT	Learning rate	$5 \times 10^{-5}$
	Epochs	10
	Episodes / epoch	500

Table A.2: Model used per experiment.

Experiment	Model	$K_{\max}$
Two-node identifiable / non-identifiable	PRIM-Small	5
Three-node confounder / mediator	PRIM-Small	5
Finetuning ablation (sinusoidal, far OOD)	PRIM-Medium	10
Finetuning ablation (NN, near OOD)	Medium	10
Finetuning ablation (NN, near OOD)	PRIM-Medium	10
Multi-root-cause identification	PRIM-Medium	10
Scalability (20–100 nodes)	PRIM-Large	100
PetShop	PRIM-Large	100
CausRCA	PRIM-Large	100
Inference time benchmark	PRIM-Large	100

Table A.3: Compute requirements. Epochs serve solely as a logging mechanism.

Component	Parameters	Hardware	Wall time	GPU-hrs
Small model	4,015,873	4×A100-80GB	5h 57m	≈ 23.8
Medium model	4,017,473	4×A100-80GB	5h 58m	≈ 23.9
Large model	4,046,273	8×A100-80GB	6h 54m	≈ 55.2
PetShop FT	—	1×A100	121 s	≈ 0.03
CausRCA FT	—	1×A100	258 s	≈ 0.07
Evaluation	—	1×A100	—	≈ 1.0
<b>Total (reported)</b>				≈ 104
<b>Total (incl. trials)</b>				≈ 620

## D Additional Results

### D.1 Identifiability in the Two-Node Case

We evaluate on a two-node graph with a single root cause, following Dhir et al. [8] with both identifiable and non-identifiable [12] linear Gaussian model posteriors. This serves as a sanity check as we expect that PRIM can recover the root cause regardlessly of the identifiability of the graph from observations. Since the Bayesian posterior assigns low probability to graphs incompatible with  $m$  and  $\mathcal{D}^{\text{int}}$ , the true root cause remains identifiable even when observational data alone is insufficient.

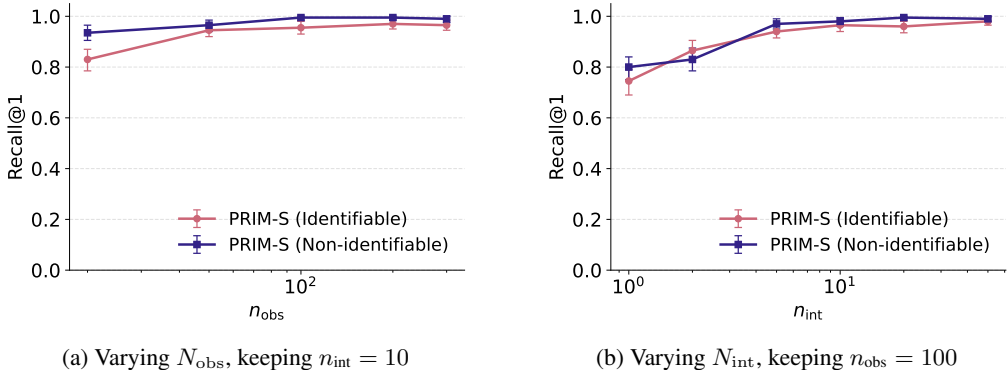


Figure C.1: Two-node identifiable vs. non-identifiable graph scenario.

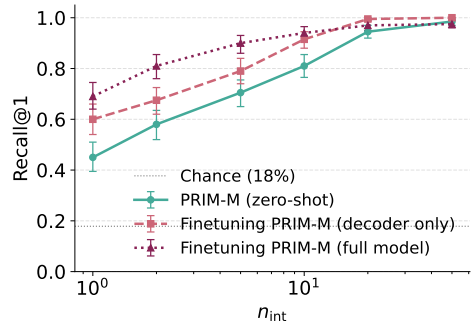
As shown in Figure C.1, PRIM correctly identifies the root cause even when the causal graph is non-identifiable from observational data alone. Performance improves monotonically with both  $N_{\text{obs}}$  and  $N_{\text{int}}$ , showing that additional observational context and more anomalous samples both improve identification. This is exactly what we would our model expect to do since we should see identifiability regardless of the fact if the graph is recoverable from observational data alone or not and the two setting should have no different results.

### D.2 Finetuning

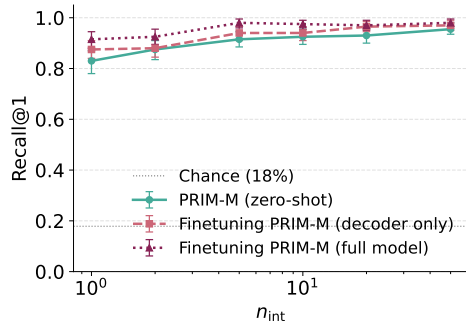
We evaluate the benefit of finetuning and the choice of finetuning variants across two out-of-distribution settings. In both cases we use random DAGs with 3–10 nodes and sweep over the number of interventional samples  $n_{\text{int}}$ , holding  $n_{\text{obs}} = 100$  fixed. In both settings finetuning uses AdamW with learning rate  $5 \times 10^{-5}$ , weight decay 0.01, 10 epochs of 500 episodes each, and  $n_{\text{obs}} = 100$  fixed. They both use  $k_{\text{max}} = 10$

*Sinusoidal* (far OOD): structural equations of the form  $f(x) = a \sin(bx + c)$  with randomly sampled parameters, entirely absent from the meta-training prior, and an intervention strength of  $2\times$  (vs.  $3\times$  during training). *NN equations* (near OOD): the same NN equation family as training but with a reduced intervention strength of  $1.5\times$  (vs.  $3\times$  during training), weakening the  $\Delta$  signal while keeping the functional form in-distribution. Three conditions are compared: zero-shot (no finetuning), decoder-only finetuning (backbone frozen), and full-model finetuning (all parameters updated). Finetuning in both cases uses synthetic data drawn from the respective target distribution.

As shown in Figure C.2, finetuning consistently reduces the number of interventional samples needed to achieve high recall, with the largest gains at small  $n_{\text{int}}$ . For the far-OOD sinusoidal setting (Figure C.2a), all three conditions are clearly separated: full-model finetuning achieves  $\approx 0.70$  recall at  $n_{\text{int}} = 1$  versus  $\approx 0.45$  for zero-shot, with decoder-only falling between the two. This indicates that the backbone itself needs to adapt to the novel functional form, and updating all parameters is beneficial. For the near-OOD NN setting (Figure C.2b), zero-shot performance is already high ( $\approx 0.83$  at  $n_{\text{int}} = 1$ ) despite the reduced intervention strength, and decoder-only finetuning nearly matches full-model finetuning across the entire sweep. This is consistent with the backbone already producing well-calibrated embeddings for the in-distribution functional form; only the mapping from  $\Delta$  to root-cause logits requires adaptation.



(a) Sinusoidal equations (far OOD)



(b) Weak-signal NN equations (near OOD)

Figure C.2: Recall@1 vs.  $n_{int}$  at fixed  $n_{obs} = 100$  for three finetuning conditions. Finetuning uses synthetic data from the target distribution. Error Bars show 90% bootstrap confidence intervals.

### D.3 Additional Results Confounder Mediator

Table C.1: Performance for Neural Network (NN) and Gaussian Process (GP) data across sample sizes ( $n_{\text{int}} = 10$  throughout). Values shown as mean [90% CI]. **Bold** indicates the best result per row overall; **blue** indicates the best result per row among graph-not-given methods.

(a)  $n_{\text{obs}} = 20$

data type	graph type	graph given		graph not given			
		traversal (true)	circa (true)	$\varepsilon$ -diag	rcd	corr	PRIM
NN	conf.	<b>0.960</b> [0.930, 0.990]	0.820 [0.750, 0.880]	<b>0.900</b> [0.840, 0.940]	0.680 [0.610, 0.760]	0.580 [0.500, 0.650]	0.750 [0.700, 0.795]
	med.	0.980 [0.960, 1.000]	<b>1.000</b> [1.000, 1.000]	0.820 [0.760, 0.880]	0.790 [0.730, 0.860]	0.620 [0.540, 0.690]	<b>0.880</b> [0.845, 0.920]
GP	conf.	<b>0.940</b> [0.900, 0.970]	0.770 [0.700, 0.840]	<b>0.850</b> [0.790, 0.900]	0.690 [0.610, 0.770]	0.540 [0.450, 0.620]	0.825 [0.780, 0.870]
	med.	0.940 [0.900, 0.980]	<b>0.970</b> [0.940, 0.990]	0.770 [0.700, 0.830]	0.660 [0.590, 0.740]	0.620 [0.550, 0.700]	<b>0.880</b> [0.840, 0.920]

(b)  $n_{\text{obs}} = 50$

data type	graph type	graph given		graph not given			
		traversal (true)	circa (true)	$\varepsilon$ -diag	rcd	corr	PRIM
NN	conf.	<b>0.990</b> [0.970, 1.000]	0.880 [0.830, 0.930]	0.850 [0.790, 0.910]	0.800 [0.740, 0.860]	0.410 [0.330, 0.490]	<b>0.885</b> [0.850, 0.920]
	med.	<b>0.980</b> [0.950, 1.000]	0.970 [0.940, 0.990]	0.860 [0.810, 0.910]	<b>0.920</b> [0.870, 0.960]	0.530 [0.440, 0.610]	0.905 [0.870, 0.935]
GP	conf.	<b>1.000</b> [1.000, 1.000]	0.780 [0.710, 0.840]	<b>0.840</b> [0.780, 0.890]	0.740 [0.660, 0.810]	0.540 [0.460, 0.620]	0.770 [0.720, 0.815]
	med.	<b>1.000</b> [1.000, 1.000]	0.960 [0.930, 0.990]	0.830 [0.770, 0.890]	<b>0.880</b> [0.820, 0.930]	0.420 [0.340, 0.500]	0.875 [0.835, 0.910]

(c)  $n_{\text{obs}} = 100$

data type	graph type	graph given		graph not given			
		traversal (true)	circa (true)	$\varepsilon$ -diag	rcd	corr	PRIM
NN	conf.	<b>1.000</b> [1.000, 1.000]	0.810 [0.740, 0.870]	0.850 [0.790, 0.900]	0.840 [0.790, 0.900]	0.460 [0.370, 0.530]	<b>0.925</b> [0.895, 0.955]
	med.	<b>1.000</b> [1.000, 1.000]	<b>1.000</b> [1.000, 1.000]	0.890 [0.830, 0.940]	0.970 [0.940, 1.000]	0.580 [0.500, 0.660]	<b>0.970</b> [0.950, 0.990]
GP	conf.	<b>0.990</b> [0.970, 1.000]	0.810 [0.740, 0.870]	0.790 [0.720, 0.860]	0.820 [0.750, 0.880]	0.580 [0.510, 0.660]	<b>0.860</b> [0.815, 0.895]
	med.	0.980 [0.960, 1.000]	<b>1.000</b> [1.000, 1.000]	0.810 [0.740, 0.870]	0.870 [0.810, 0.920]	0.520 [0.440, 0.600]	<b>0.915</b> [0.880, 0.945]

(d)  $n_{\text{obs}} = 200$

data type	graph type	graph given		graph not given			
		traversal (true)	circa (true)	$\varepsilon$ -diag	rcd	corr	PRIM
NN	conf.	<b>1.000</b> [1.000, 1.000]	0.820 [0.760, 0.880]	0.820 [0.760, 0.880]	0.870 [0.820, 0.920]	0.430 [0.350, 0.510]	<b>0.900</b> [0.865, 0.935]
	med.	<b>0.990</b> [0.970, 1.000]	<b>0.990</b> [0.970, 1.000]	0.860 [0.800, 0.920]	<b>0.960</b> [0.920, 0.990]	0.590 [0.520, 0.680]	0.955 [0.930, 0.975]
GP	conf.	<b>1.000</b> [1.000, 1.000]	0.870 [0.810, 0.920]	0.770 [0.700, 0.830]	0.720 [0.640, 0.790]	0.440 [0.360, 0.520]	<b>0.850</b> [0.810, 0.885]
	med.	<b>1.000</b> [1.000, 1.000]	<b>1.000</b> [1.000, 1.000]	0.830 [0.770, 0.890]	0.900 [0.850, 0.950]	0.450 [0.380, 0.520]	<b>0.920</b> [0.885, 0.950]

(e)  $n_{\text{obs}} = 300$

data type	graph type	graph given		graph not given			
		traversal (true)	circa (true)	$\varepsilon$ -diag	rcd	corr	PRIM
NN	conf.	<b>0.990</b> [0.970, 1.000]	0.870 [0.810, 0.920]	0.750 [0.680, 0.820]	0.820 [0.750, 0.880]	0.550 [0.460, 0.620]	<b>0.910</b> [0.875, 0.940]
	med.	<b>1.000</b> [1.000, 1.000]	0.990 [0.970, 1.000]	0.880 [0.830, 0.930]	0.920 [0.870, 0.960]	0.550 [0.470, 0.630]	<b>0.975</b> [0.955, 0.990]
GP	conf.	<b>1.000</b> [1.000, 1.000]	0.760 [0.690, 0.820]	0.840 [0.780, 0.900]	0.740 [0.660, 0.810]	0.410 [0.330, 0.490]	<b>0.860</b> [0.815, 0.900]
	med.	0.970 [0.940, 1.000]	<b>0.980</b> [0.950, 1.000]	0.810 [0.740, 0.870]	0.900 [0.850, 0.950]	0.510 [0.430, 0.590]	<b>0.925</b> [0.895, 0.955]

#### D.4 Additional Results Different Node Sizes

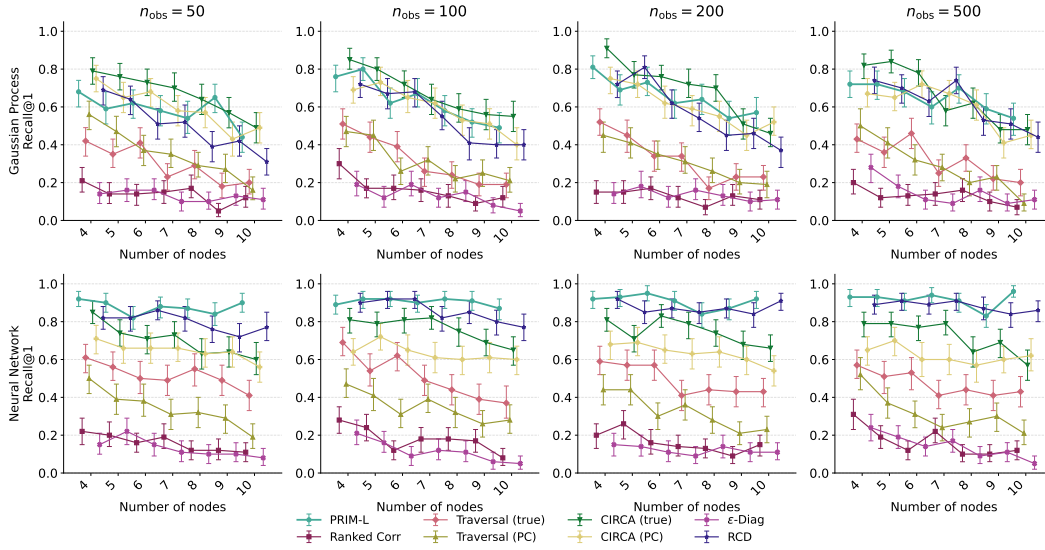


Figure C.3: Recall@1 vs. number of nodes across all observation sizes ( $n_{obs} \in \{50, 100, 200, 500\}$ ,  $n_{int} = 10$ ). Rows correspond to data generating process (Gaussian Process and Neural Network); columns correspond to number of observations. For smaller Model (3 to 10 Nodes)

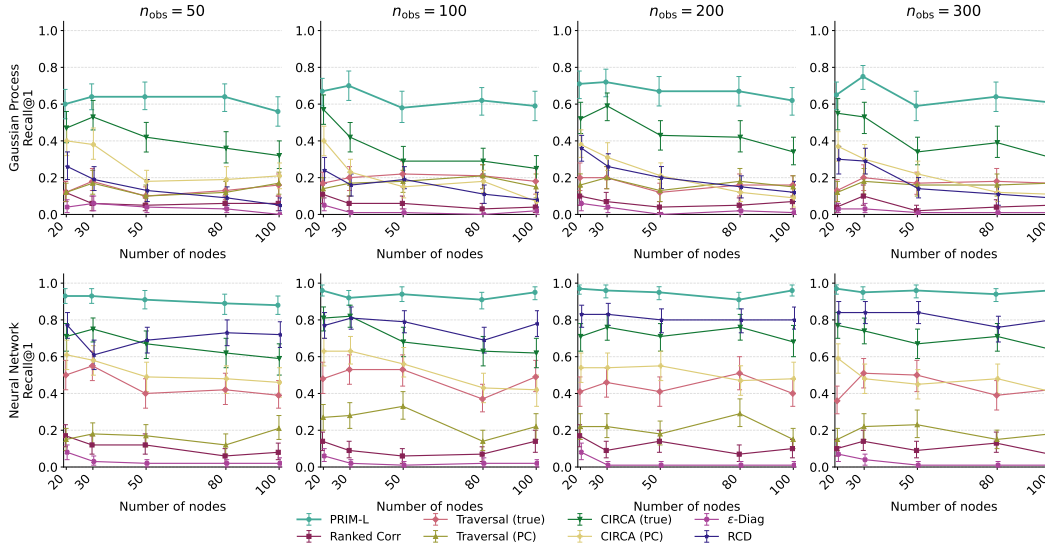


Figure C.4: Recall@1 vs. number of nodes across all observation sizes ( $n_{obs} \in \{50, 100, 200, 500\}$ ,  $n_{int} = 10$ ). Rows correspond to data generating process (Gaussian Process and Neural Network); columns correspond to number of observations. For large Model trained on (17 - 100 Nodes)

## D.5 Inference Time

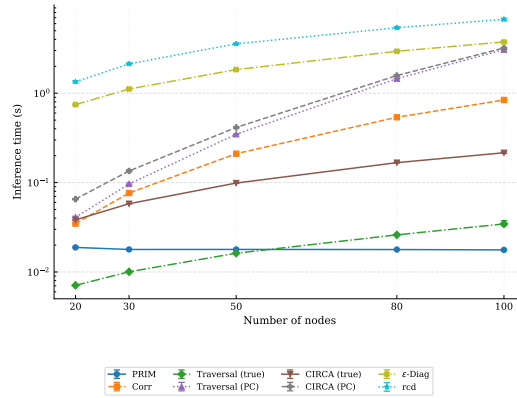


Figure C.5: Inference time for different node sizes for different methods  $n_{\text{obs}} = 100$ ,  $n_{\text{int}} = 20$

Table C.2: PRIM inference time on a MacBook (4,046,273 parameters). Mean and 90% bootstrap CI over 100 episodes per configuration ( $n_{\text{obs}} = 100$ ,  $n_{\text{int}} = 20$ ).

Device	$K$	Mean (ms)	CI <sub>lo</sub> (ms)	CI <sub>hi</sub> (ms)
CPU	20	262.9	262.5	263.5
	30	265.9	265.4	266.5
	50	274.7	273.9	275.4
	80	281.7	281.1	282.3
	100	289.1	288.0	290.2
MPS (Apple GPU)	20	36.5	35.3	38.6
	30	35.3	35.3	35.4
	50	35.6	35.6	35.7
	80	35.9	35.9	35.9
	100	35.9	35.9	36.0

### D.6 Recall@1 For Petshop

Table C.3: Top-1 recall of the RCA methods measuring the accuracy of identifying the correct root-cause node. Results marked with \* are taken from Hardt et al. [13]; † denotes our methods. **Bold** indicates the best result per row overall; **blue** indicates the best result per row among graph-not-given methods.

traffic scenario	metric	graph given			graph not given				
		traversal*	circa*	counter-factual*	$\epsilon$ -diag.*	rcd*	corr*	PRIM†	PRIM FT†
low	latency	<b>0.57</b>	0.36	0.36	0.00	0.07	<b>0.43</b>	0.10	0.00
low	availability	0.50	0.42	0.00	0.00	0.58	0.75	0.63	<b>0.88</b>
high	latency	0.57	0.50	0.57	0.00	0.00	<b>0.64</b>	0.00	0.10
high	availability	0.33	0.00	0.00	0.00	0.00	<b>0.83</b>	0.00	0.00
temporal	latency	<b>1.00</b>	0.75	0.38	0.12	0.25	0.62	<b>0.67</b>	0.50
temporal	availability	0.38	0.38	0.00	0.00	0.50	<b>0.62</b>	0.33	0.50
average		0.56	0.40	0.22	0.02	0.23	<b>0.65</b>	0.29	0.33

### D.7 Additional Benchmarks on CausRCA

Table C.4: MAP@3 for Unsupervised RCA algorithms. †Ours. **Bold** indicates best result per row overall; **blue** indicates best result per row among graph-not-given methods.

Dataset		graph given		graph not given			
		Traversal	CIRCA	$\epsilon$ -Diag	RCD	PRIM†	PRIM-FT†
Coolant	Full	0.00	0.20	0.00	0.01	0.55	<b>0.63</b>
	Sub	0.00	0.21	0.00	0.41	0.75	<b>0.96</b>
Hydraulics	Full	0.00	0.17	0.00	0.08	0.61	<b>0.66</b>
	Sub	0.00	0.20	0.02	0.21	0.87	<b>0.91</b>
Probe	Full	0.00	0.01	<b>0.06</b>	0.01	0.00	0.00
	Sub	0.00	0.23	0.29	0.14	0.18	<b>0.45</b>
Mean ( $M$ )	Full	0.00	0.12	0.02	0.04	0.39	<b>0.43</b>
	Sub	0.00	0.21	0.11	0.24	0.61	<b>0.77</b>